AFOSR-TR- 94 0238

AD-A278 271

Approved for public release; distribution unlimited.

APPROVED FOR PUBLIC RELEASE
DISTRIBUTION UNLIMITED

RESEARCH IN THE OPTICAL SCIENCES

Final

~~Annual~~ Technical Report Prepared for
Air Force Office of Scientific Research
Joint Services Optics Program

October 1, 1992, through November 30, 1993

Contract F49620-91-C0009

DTIC
ELECTE
APR 20 1994
S F D

Richard C. Powell, Director
Optical Sciences Center
University of Arizona
Tucson, Arizona 85721

February 1994

94-11896

94 4 19 022

unclassified
SECURITY CLASSIFICATION OF THIS PAGE

REPORT DOCUMENTATION PAGE

Form Approved
OMB No. 0704-0188

1a. REPORT SECURITY CLASSIFICATION unclassified	1b RESTRICTIVE MARKINGS
2a. SECURITY CLASSIFICATION AUTHORITY	3. DISTRIBUTION / AVAILABILITY OF REPORT approved for public release; distribution unlimited
2b. DECLASSIFICATION / DOWNGRADING SCHEDULE	
4. PERFORMING ORGANIZATION REPORT NUMBER(S)	5. MONITORING ORGANIZATION REPORT NUMBER(S) AFOSR F59620-91-C0009 AFOSR-TR- 94 0238
6a. NAME OF PERFORMING ORGANIZATION Optical Sciences Center 6b. OFFICE SYMBOL (If applicable)	7a. NAME OF MONITORING ORGANIZATION ONRRR
6c. ADDRESS (City, State, and ZIP Code) University of Arizona Tucson, Arizona 85721	7b. ADDRESS (City, State, and ZIP Code) University of New Mexico Bandelier Hall West Albuquerque, NM 87131
8a. NAME OF FUNDING / SPONSORING ORGANIZATION JSOP (AFOSR) 8b. OFFICE SYMBOL (If applicable)	9. PROCUREMENT INSTRUMENT IDENTIFICATION NUMBER ~~AFOSR~~ F49620-91-C0009
8c. ADDRESS (City, State, and ZIP Code) Air Force Office of Scientific Research Bolling Air Force Base Washington, DC 20332-6448	10. SOURCE OF FUNDING NUMBERS PROGRAM ELEMENT NO. 61102F; PROJECT NO. 2301; TASK NO CS; WORK UNIT ACCESSION NO

11. TITLE (Include Security Classification)
Research in the Optical Sciences

12. PERSONAL AUTHOR(S)
Richard C. Powell

13a. TYPE OF REPORT	13b. TIME COVERED	14. DATE OF REPORT (Year, Month, Day)	15. PAGE COUNT
~~annual~~ Final	FROM 10/1/92 TO 11/30/93	1994 February 28	58

16. SUPPLEMENTARY NOTATION

17. COSATI CODES			18. SUBJECT TERMS (Continue on reverse if necessary and identify by block number)
FIELD	GROUP	SUB-GROUP	optical sciences

19. ABSTRACT (Continue on reverse if necessary and identify by block number)

This report discusses research progress in the optical sciences, including the areas of: Monte Carlo simulation of multiple quantum well infrared detectors; wide field-of-view micro-optics; optical elements for X-UV wavelengths; fundamental physics of MBE heterostructures; MBE growth of novel semiconductor heterostructures; optical nonlinearities in low-dimensional semiconductor structures; carrier relaxation studies in semiconductor lasers and in novel GaAs quantum-well structures; spectral hole burning and instabilities in semiconductor lasers; surface characterization of semiconductor structures; propagation of short optical pulses in passive and active nonlinear all-optical switches; and atom optics.

DTIC QUALITY INSPECTED

20. DISTRIBUTION / AVAILABILITY OF ABSTRACT	21 ABSTRACT SECURITY CLASSIFICATION
☒ UNCLASSIFIED/UNLIMITED ☐ SAME AS RPT. ☐ DTIC USERS	unclassified
22a. NAME OF RESPONSIBLE INDIVIDUAL ~~Sandra L. Singer~~ Schlossberg	22b TELEPHONE (Include Area Code) / 22c. OFFICE SYMBOL NE

DD Form 1473, JUN 86 Previous editions are obsolete

SECURITY CLASSIFICATION OF THIS PAGE
unclassified

CONTENTS

Accesion For
NTIS CRA&I ☑
DTIC TAB ☐
Unannounced ☐
Justification .....
By .....
Distribution /
Availability Codes
Dist | Avail and / or Special
A-1

EXECUTIVE SUMMARY

This report covers work accomplished at the Optical Sciences Center during the period from October 1992 through November 1993, and supported by the Joint Services Optics Program. The report describes results obtained in 11 research projects spanning the field of optics from fundamental quantum optics theory to applied optical engineering. These projects supported more than 24 graduate students and several post-doctoral associates, and resulted in more than 127 publications during this year. The research involved collaborations at a number of Department of Defense and Department of Energy laboratories including the Army Center for Night Vision and Electro-Optics, Rome Air Development Center, Air Force Phillips Laboratory, Lawrence Livermore National Laboratory, and Sandia National Laboratory.

Some of the highlights of the research are listed below and the details of the work are given in the following sections.

- A simulation model was developed for a multiple quantum well infrared photodetector that enhances the ability to design and optimize new detector structures.
- An improved near-field scanning optical microscope was developed and tested.
- High quality single-crystal layers of beryllium were grown on germanium by molecular beam epitaxy (MBE) techniques.
- The properties of vertical-cavity surface-emitting lasers (VCSELs) with injection seeding were characterized.
- Photon correlation measurements were used to show that there is no *thresholdless* laser.
- Many-body effects for two-component plasmas were characterized for quantum well structures.
- Femtosecond spectral hole-burning techniques were employed to characterize the relaxation of nonequilibrium carriers in semiconductors.
- The properties of microcavity lasers were analyzed and found to be significantly different than normal lasers.
- Scanning tunneling microscope techniques were developed to characterize semiconductor optics on a nanosecond time scale with nanometer resolution.
- A figure of merit was developed for the use of quantum dots as all optical switches and applied to a variety of materials.
- Theoretical models were developed to characterize quantized atomic motion in one-, two-, and three-dimensional optical lattices.

Richard C. Powell, Director
Optical Sciences Center
February 1994

MONTE CARLO SIMULATION OF MULTIPLE QUANTUM WELL INFRARED DETECTOR

E.L. Dereniak, V. Sankaran and A. Käkkäinen

PUBLICATIONS

D. Perry and E. Dereniak, "Linear theory of nonuniformity correction in infrared staring sensors," Opt. Eng. 32, 1854 (1993).

T. Graeve and E. Dereniak, "Power dissipation on frame-transfer charge-couple devices," Opt. Eng. 32, 904 (1993).

SCIENTIFIC PERSONNEL

Dave Perry
Vanitha Sankaran
Anna Käkkäinen

RESEARCH FINDINGS

A proposal for a simulation model of a multiple quantum well infrared photodetector (MQWIP) is presented. Although the theory of MQWIPs is well studied, very little simulation results of MQWIP have been published. Besides understanding the operation of MQWIPs, the simulation model is a useful tool for designing and optimizing new detector structures.

The theoretical analysis is based on Boltzmann transport equation, which is solved with Monte Carlo (MC) simulation combined with a Poisson equation solver. The MC method applied to charge transport in detector consists of the simulation of carriers in a given electric field and scattering mechanisms. The approach is semiclassical electron trajectories and quantum mechanically calculated scattering probabilities.

A widely used method of modeling semiconductor devices is the drift diffusion (DD) model, which uses phenomenological parameters such as mobility and diffusion coefficient. It assumes that the energy and momentum of the charger carriers remain close to that of an equilibrium distribution. This is a good approximation for many large-scale devices; however, in submicron range this assumption is no longer valid. For multiple quantum well (MQW) structures a more elaborate method is asked for. MC methods give self-consistent solutions for the Boltzmann transport equation which gives a better description of multiple quantum well devices.

Monte Carlo Simulation

The MC method applied to charge transport in semiconductors consists of simulating one or more carriers in a given electric field and scattering mechanism. The simulation starts with approximating the electron charge density ρ_{el}. This could be calculated, for example, with the DD-model. This is used as input to the Poisson equation.

$$\nabla^2 E = \rho_{tot} \tag{1}$$

where ρ_{tot} is the total charge density from electrons and ionized donors. The MC part consists of simulated electron flights: one electron is given initial conditions with wavevector **k**. Then the duration of the first free flight is chosen with a probability distribution determined from the scattering probabilities. By keeping statistics of the electron motion (i.e., how much time it spends in each lattice point), it is possible to estimate the charge density inside the detector. After many simulated trajectories, the average electron charge density ρ_{el} is calculated and fed back to solve the Poisson Eq. (1) again. The

entire process is repeated until a self-consistency between the electric field and the charge density is acquired.

During the free flight the electric fields are acting according to the relation

$$\hbar \mathbf{k} = -e\mathbf{E} \tag{2}$$

and kept constant. All the quantities of interest, velocity, energy, etc., are recorded. A scattering mechanism is chosen at the end of the free flight. New state of k is calculated according to the chosen scattering mechanism and it becomes the initial state for the new free flight.

Since the electron scattering probabilities are functions of electron energies, calculation of the flight durations would be difficult and time consuming. To overcome this, the self-scattering scheme is introduced. The maximal scattering rate Γ is used as a constant to produce flight durations. After the flight, it is decided which physical scattering mechanism to use or whether to scatter at all. In the latter case, it is said that the electron underwent a self scattering. If the scattering rates vary over space and k-values a lot, most of the simulated scattering events are self-scattering. This slows the simulation considerably and extensive algorithm development has been done to find efficient ways to reduce the amount of self scattering.

The result of the calculation becomes more precise as the simulation goes on and the simulation ends when the quantities of interest are known with the desired precision.

The MC method simulates the dynamics of a single electron inside the crystal, which makes it similar to experimental techniques. In fact, it can be considered as a simulated experiment.

Scattering Rates

For the two-dimensional (2D) systems the scattering rates are calculated as for the bulk, for lack of a better model. Scattering rate calculations usually rely on first-order perturbation theory. Fermi's golden rule is a constant rate of transition. Scattering in three dimensions (3D) is considered as well-understood theory, and comprehensive presentations can be found in the literature.

Usually the following scattering mechanisms are included in semiconductor device modeling: acoustic phonons, optical phonons, ionized impurities, interface scattering, and carrier-carrier scattering. In high-temperature region (even in room temperature) optical phonon scattering is the most important. In low temperatures the ionized impurity scattering dominates.

Absorption

The photon absorption in 2D was solved already in 1957 by Elliott:

$$\alpha^{2D}(\omega) = \frac{2\pi\omega|d_{cv}|^2}{n_0 c L_z}\left[\frac{2m^*}{\hbar^2}\right]\left[\sum_{n=1}^{\infty}\frac{4E_B}{\left[n-\frac{1}{2}\right]^3}\,\delta\left[\hbar\omega - E_g^{2d} + \frac{E_B}{\left(n-\frac{1}{2}\right)^2}\right] + \theta\left(\hbar\omega - E_g^{2d}\right)\frac{e^{\Delta}}{\cosh\Delta}\right] \tag{3}$$

where E_B is the three-dimensional exciton Rydberg given by $E_B = e^4 m^*/2\epsilon_0^2\hbar^2$. The first term in the bracket corresponds to the excitonic lines. The excitonic absorption is of great importance in 2D systems because the binding energies are four times stronger than in bulk. However, excitons are not of interest in detector operation because they do not produce photoelectrons.

The absorption constant α^{2D} can be calculated by solving the transition probability matrix d_{cv}, where c(v) refers to conduction (valence) band.

The from-first principles calculation of the probability matrix d_{ν} is rather complicated and needs super-computer power. However, since the steady-state MC calculation already predicts the charge density, we can use this to determine the absorption (up to a constant), because it is proportional to the charge distribution. The constant can be fixed using experimental data of the absorption rate.

The absorption in 2D structures depends on polarization. Only the light polarized perpendicular to the layers is absorbed.

Simulation

The simulation of MQWIP can be divided in two parts: steady-state (or carrier-transportation) and absorption simulation. Figures 1 and 2 are corresponding flow charts. The purpose of the steady-state simulation is to calculate how the electrons and doped ions are distributed in the medium (electric field), how fast the electrons reach the collector (mean velocity) and how many electrons reach the collector (photo-conductive gain). From the charge distribution the absorption coefficient $\alpha(z)$, where z is the spatial coordinate, can be determined up to a constant.

In absorption simulation the place z of absorption is determined. The initial energy and polarization is given to the photon entering the detector. Probabilistic criteria are used to determine if the photon is reflected from the surface. If not, a statistical distribution calculated from the absorption equation $e^{-\alpha(z)z}$ is used to determine if the photon is absorbed to the first quantum well. The same is repeated for the following wells until the photon is absorbed or until it reaches the collector. Combining the absorption rate with the simulated transport properties of the detector, the pulse shape and quantum efficiency can be determined.

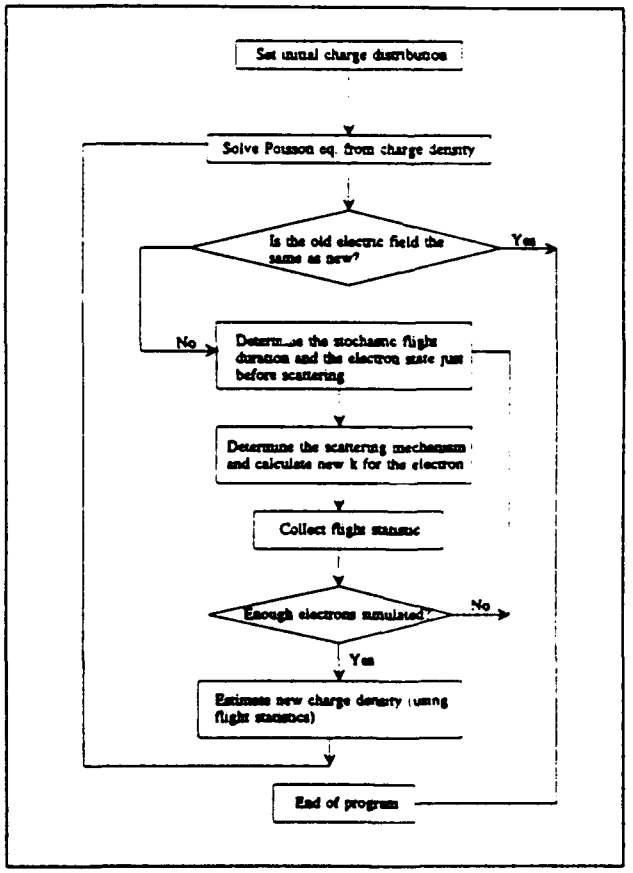

Figure 1. Flowchart of the steady-state simulation.

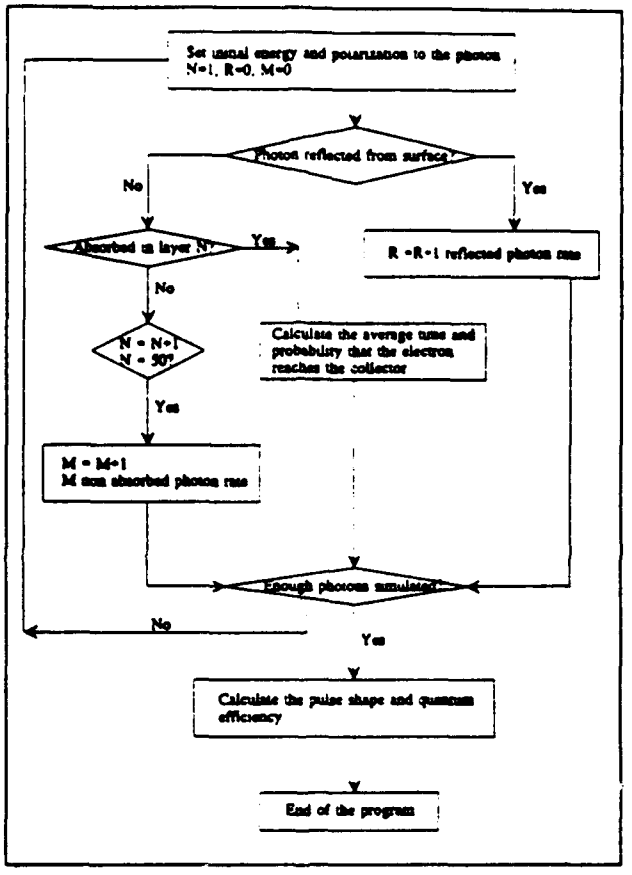

Figure 2. Flowchart of the absorption simulation.

WIDE FIELD-OF-VIEW MICRO-OPTICS

T.D. Milster

PUBLICATIONS

F.F. Froehlich, T.D. Milster and J.L. Kann, "A near-field scanning optical microscope for analysis of magneto-optic media," poster presentation, Joint International Symposium on Optical Memory and Optical Data Storage, Maui, Hawaii, July 1993.

J.L. Kann, T.D. Milster, F. Froehlich, R.W. Ziolkowski and J. Judkins, "Numerical analysis of a two dimensional near-field probe," poster presentation, Second International Conference on Near Field Optics, Raleigh, North Carolina, October 1993.

J.L. Kann, T.D. Milster, F. Froehlich, R.W. Ziolkowski and J. Judkins, "Numerical analysis of a two dimensional near-field probe," accepted for publication, J. Ultramicroscopy, June 1994.

RESEARCH FINDINGS

Experimental Work

We are continuing to develop our second-generation near-field scanning optical microscopy (NSOM) instrument that we reported on previously. The current configuration of the instrument is shown in Fig. 1, and is similar to the design described in detail in last year's report. The figure shows the head assembly of the microscope consisting of optical and mechanical hardware with the servo system. We have interfaced our head assembly to a commercial atomic force microscope (AFM) (not shown) that was donated to the project by WYKO Inc., Tucson, Arizona. The AFM is used to control the raster scanning of the sample, and to acquire, display and process the data. Our microscope unfortunately is still not fully operational due to difficulties encountered with the servo system that maintains the probe tip-to-sample spacing (10 nm to 40 nm) required for high spatial resolution. The servo system represents a significant engineering challenge, and we have solved numerous hardware problems during the past year that were hindering its operation. However, the sample stage continues to be a problem due to its poor frequency response and resonance behavior. This stage is a complex piezoelectrically driven flexure design that provides raster scanning of the sample in x and y, and servo correction in z. It is our opinion that the electro-mechanical performance of our servo cannot be further improved to an adequate level using this stage and our current hardware configuration. Therefore, we are planning to modify the head of our WYKO AFM for use as a NSOM microscope. The WYKO unit is a proven design, and its use will eliminate the problems we are experiencing with our mechanics and piezoelectric positioners. The cost of taking this approach is sacrificing the excellent scan linearity afforded by the flexure sample stage, and some loss of system flexibility. We anticipate carrying out the modifications to the WYKO unit during the next funding cycle.

We are studying the servo system in detail to quantify its sensitivity and to understand its performance limitations. The servo system used in our microscope is based on sensing the atomic forces between the tip and sample surface to maintain the tip-to-sample spacing. A small dither oscillation is applied to the tip (typically several nanometers), and the amplitude of the dither decreases as the tip comes close to the surface and experiences the attractive van der Waals forces of the surface atoms. The sensing of this minute dither amplitude is a critical part of the servo system. The sensing is performed by diffracting light from a focused HeNe laser off the tip and by differentially detecting the resultant modulation of the diffraction pattern with a photodiode. We developed this technique simultaneously, but independently, with other NSOM research groups. This technique is superior to the scheme we

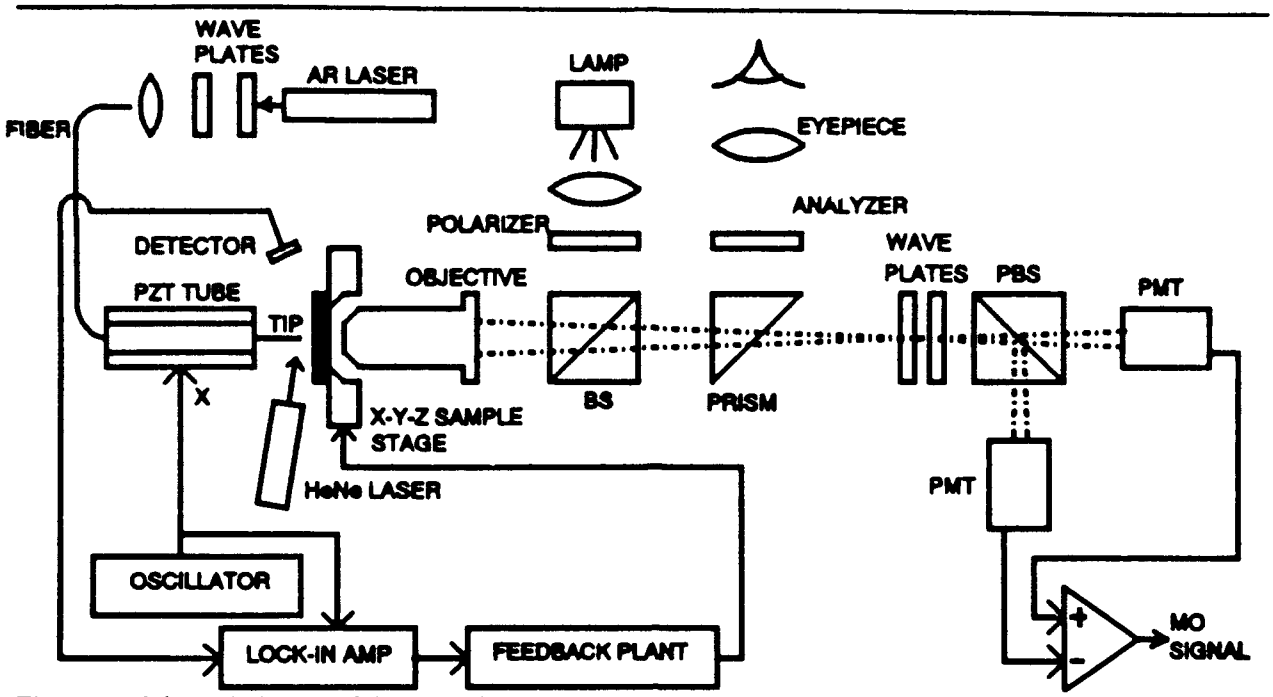

Figure 1. Schematic layout of the NSOM microscope head showing optics, mechanics and servo system.

originally proposed in last year's report, which involves imaging the dithering tip to a pinhole. We are conducting a theoretical and experimental analysis of this technique for publication, as no such analysis has yet appeared in the literature. Figure 2 shows theoretical calculations of the differential signal vs lateral tip offset with defocus as a parameter. The strength of the signal is proportional to the slope of a given curve. Therefore, the model indicates that the sensitivity is enhanced by defocusing the tip from the laser spot, and defocusing makes the signal less dependent on tip offset.

Modeling Work

A rigorous electromagnetic model is being used to study both the near-zone (within 100 nm of the aperture) and far-zone (out to hundreds of microns) fields associated with a typical NSOM structure. A two-dimensional finite-difference-time-domain (FDTD) code is used to find the steady-state time-averaged fields in and around a sub-wavelength aperture. The FDTD code discretizes the problem in both time and space (creating a grid), and then solves Ampere's and Faraday's equations within the grid at each time step. The code runs for 16 optical cycles, and data is time averaged over the last cycle. This code also allows us to study the effects of placing various multi-layer structures in proximity to the aperture. An angular spectrum technique is then applied to propagate the field components from the FDTD code to the far-zone.

An example output from the model is shown in Fig. 3. The figure shows a perspective plot of the normalized electric field intensity emanating from a slit aperture. In the model, a normally incident TM-polarized plane wave (λ = 500 nm) is used to illuminate a 100 nm wide slit in a metal screen of infinite conductivity. The metal screen is 25 nm thick, and the medium surrounding it is air. The field enhancement near the aperture is caused by the sharp corners of the slit in the metal, where a large charge density accumulates. The energy past the aperture remains well collimated for a distance of approximately half the aperture width. Past this distance, it diverges linearly, similar to what is seen for a larger aperture. However, the intensity falls off exponentially, due to the fact that most of the energy transmitted through the aperture is not propagating, but evanescent.

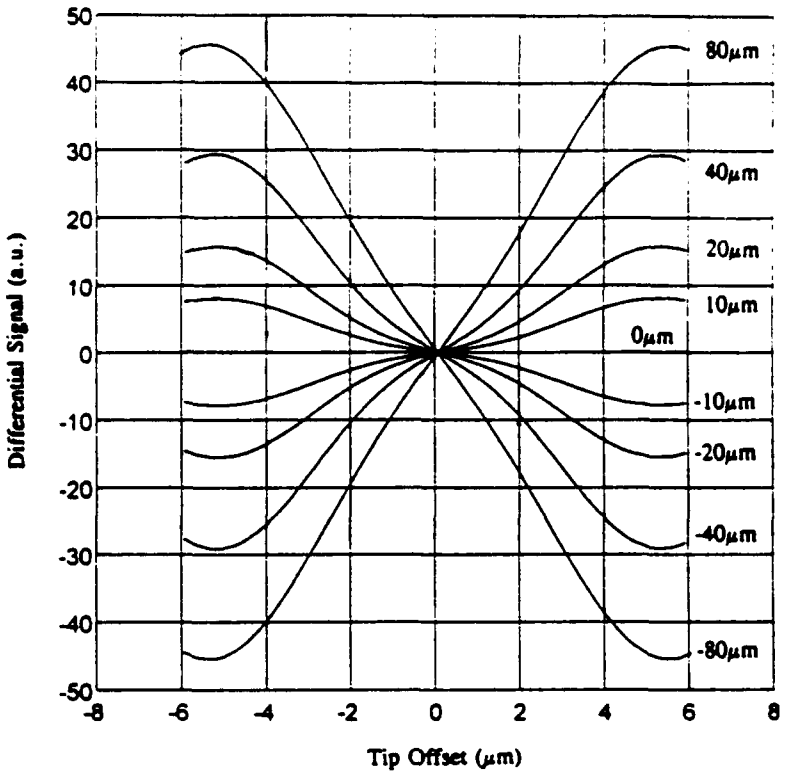

Figure 2. Plots of differential signal vs lateral tip offset with axial defocus as a parameter.

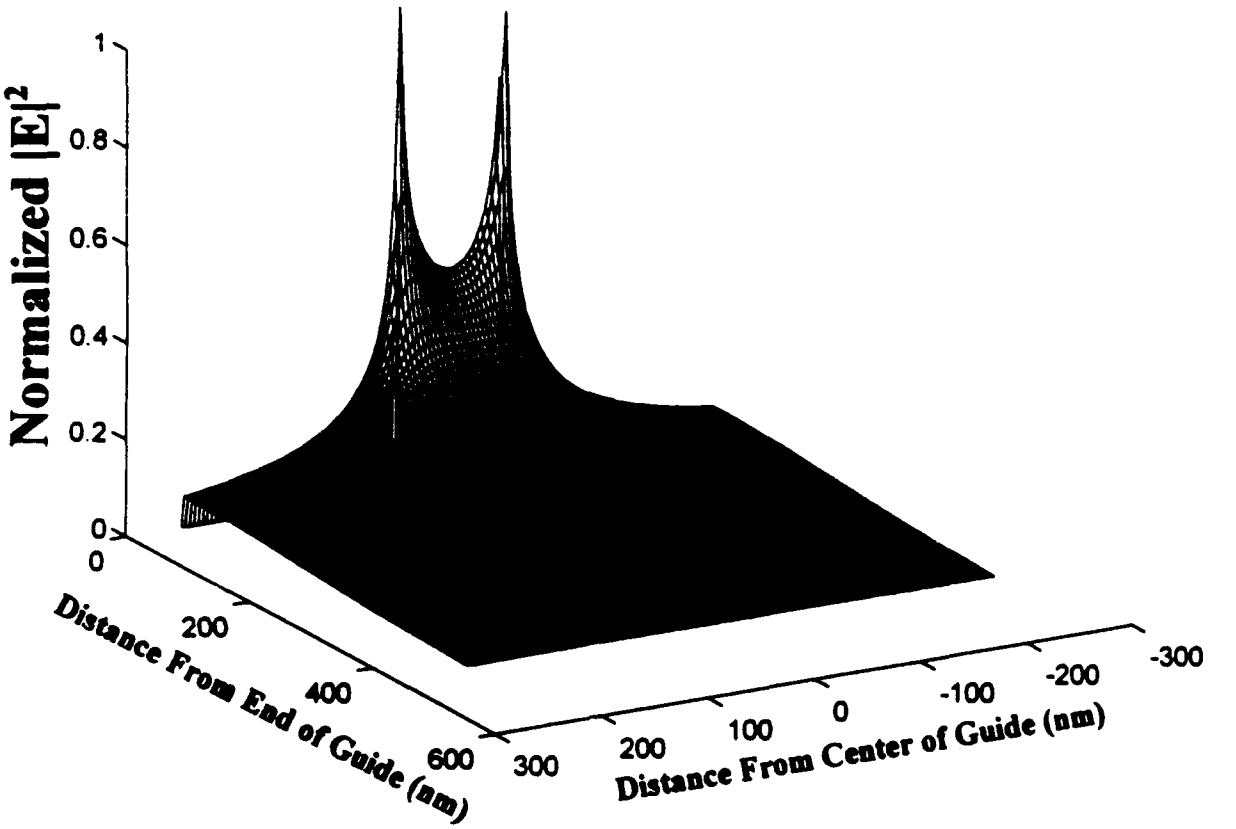

Figure 3. The normalized $|E|^2$ emanating from a slit aperture in a metal screen. The aperture is 100 nm wide and is illuminated with a normally incident TM polarized plane wave. All distances are in nm.

OPTICAL ELEMENTS FOR X-UV WAVELENGTHS

C.M. Falco and J.M. Slaughter

PUBLICATIONS

J.M. Slaughter, W. Weber, G. Güntherodt and C.M. Falco, "Quantitative auger and XPS analysis of thin films," MRS Bulletin 17, 39 (1992).

C.M. Falco, P.A. Kearney, J.A. Ruffner and J.M. Slaughter, "Structure and x-ray optical properties of MBE-grown multilayers," SPIE, Proc. 1720, (1992).

J.M. Slaughter and C.M. Falco, "Non-specular x-ray scattering from Si/Mo multilayers," SPIE, Proc. 1742, 365 (1992).

E. Chason, C.M. Falco, A. Ourmazd, E.F. Schubert, J.M. Slaughter and R.S. Williams, "Interface roughness: what is it and wow is it measured?" MRS Proc. 280, 203 (1993).

D.H. Shen, P.A. Kearney, J.M. Slaughter and C.M. Falco, "Chemical interaction at the Pd-B interface," J. Mag. and Mag. Mats., 126, 25 (1993).

C.M. Falco and J.M. Slaughter, "Characterization of metallic multilayers for x-ray optics," J. Mag. and Mag. Mats., 126, 3 (1993).

J.A. Ruffner, J.M. Slaughter, J. Eickmann and C.M. Falco, "Epitaxial growth and surface structure of (0001) Be on (111) Si," Appl. Phys. Lett. (in press).

SCIENTIFIC PERSONNEL

Judith Ruffner, Graduate Research Assistant
Patrick Kearney, Graduate Research Assistant

DEGREES AWARDED

Judith Ruffner, Ph.D., passed oral exam February 12.

RESEARCH FINDINGS

This year we continued our study of epitaxial beryllium growth using molecular beam epitaxy (MBE). We were successful in growing very high quality single-crystal beryllium on germanium (111) substrates. Our epitaxial Be films grown on Ge are even higher quality than our previous films grown on silicon (111) and sapphire. The quality of the initial Ge surface and the substrate temperature during growth are the most important variables affecting the structure of the Be film. We also have grown certain Be-Ge heterostructures.

We continued our development of non-specular x ray scattering as a multilayer characterization tool. The non-specular behavior can be understood in terms of current theories of x ray scattering from multilayers with correlated interface roughness. Detailed analysis of the evolution of interface roughness in multilayers using non-specular scattering has been carried out in collaboration with D. Stearns at Lawrence Livermore Laboratory. We have used this technique to determine the evolution of the roughness power spectral density from interface-to-interface in the multilayer film. We believe this is

the first time such detailed information about the roughness evolution in multilayers has been measured without a synchrotron source.

Beryllium Results

We have previously succeeded in growing single-crystal hcp beryllium on sapphire (001) and Si (111) substrates using MBE. During this period, we have succeeded in growing Be epitaxially on Ge (111). These films are even higher quality than the films we grew previously on sapphire and Si. The higher quality is probably due to the smaller lattice mismatch between Ge and Be, 1.0 vs. 3.1% for Be-on-Si and 3.9% for Be-on-sapphire.

Beryllium on Silicon. Table 1 summarizes the characterization results for Be grown on (111) Si. These structural parameters are discussed in more detail in our previous technical reports and our publications. We made additional samples at T=300 °C and T=400 °C to verify the high quality at 300 °C and morphology change at 400 °C. The films with the highest quality are those deposited at T=300 °C. The sample made at T=500 °C has better crystallinity, but is composed of islands rather than a continuous film. Scanning electron microscope (SEM) and atomic force microscope (AFM) images of films grown at T=400 °C, show the hexagonal island formations typical of these higher T samples. These islands are peculiar in that they are typically large (~1 μm diameter), flat-topped, roughly hexagonal islands with terraced sides topped by a small island in the center. Because the morphology changes so drastically between T=300 °C and T=400 °C, there may be a surface roughening transition in this temperature region. Further studies of the morphology as a function of deposition temperature and annealing temperature are needed to understand the driving forces behind this drastic morphological change.

Table 1. Characterization results for epitaxial beryllium films grown on Si (111) at several substrate temperatures (T). The effective thickness from ion beam analysis (d_{IBA}) is a measure of how much beryllium was deposited. Better crystalline quality is indicated by having an x-ray coherence length (L) nearer to the film thickness (d_{LAD}), and by lower values of rocking curve width ($\delta\theta$) and ion beam channeling ratio (χ).

T (°C)	d_{IBA} (Å)	d_{LAD} (Å)	L (Å)	$\delta\theta$ FWHM (deg.)	χ
100	1870±190	1630±10	920	0.38±0.02	0.73±0.02
200	1970±200	1770±10	1050	0.32±0.02	0.38±0.02
300	1700±170	1530±10	1320	0.24±0.02	0.33±0.02
400	1060±110	islands	850	0.26±0.02	0.41±0.02
500	1120±80	islands	1560	0.20±0.02	0.79±0.02

Beryllium on Germanium. Results from RHEED analysis of the Be films grown on Ge buffer layers on Si(111) indicated that the Be grows with the Be[0001] direction parallel to the Ge[111] direction. Also, the Be is oriented with Be[10$\bar{1}$0] direction parallel to the Ge[$\bar{1}$10] direction and the Be[11$\bar{2}$0] direction parallel to the Ge[2$\bar{1}$1]. In addition, a surface superstructure, probably $(\sqrt{3}x\sqrt{3})R30^\circ$, is observed on the samples with T ≥ 300 °C. X ray diffraction analysis and ion channeling results

indicate an increase in crystalline quality as T is increased. However, samples deposited at T ≥ 300 °C are visibly rough. The effects on crystalline quality and surface roughness of increasing the temperature T can be explained through surface mobility considerations. Increasing T probably results in increased mobility of the Be adatoms allowing more ordered growth. However, above T = 300 °C, the surface mobility may become great enough to favor formation of large islands. Increased defects and surface roughness may result as these islands grow together.

Analysis of RHEED patterns for Be films grown on Ge buffers on Ge(111) substrates indicate that the Be grows with the same orientation as when it is deposited on Ge buffers on Si(111) substrates. However, in the case of Be on Ge(111), we observe the surface superstructure on all samples even for those with T < 300 °C. X ray diffraction analysis and ion beam channeling show the highest crystalline quality is attained at T = 300 °C. As T increases above 300 °C or decreases below 300 °C, crystalline quality is decreased. All of the samples deposited were visibly smooth. Again, the effect on crystalline quality of increasing the temperature T may be explained in terms of adatom surface mobility, with T = 300 °C resulting in a mobility that favors highly ordered growth of smooth thin films. In addition, the crystalline quality of these films grown on Ge(111) was significantly greater than Be films grown on Ge(111) buffer layers on Si(111). We suggest that the influence of the substrate material on the crystalline quality of the Be overlayer is a result of differences in the quality of the Ge buffer layers. Atomic force microscopy and ion beam channeling reveal that the Ge buffer layers deposited on Ge(111) are of much higher crystalline quality than the buffer layers grown on Si(111). Since defects in a buffer layer tend to propagate through an overlayer, the poorer quality Ge buffers on Si most likely lead to poorer quality Be films.

Germanium on Beryllium. RHEED analysis of the Ge films grown on Be buffers on Si(111) indicate that Ge grows epitaxially for T = 425 °C, but polycrystalline for T = 300 °C. This behavior also may be explained in terms of increased Ge adatom mobility at higher temperatures. For the epitaxial samples, the Ge grows with Ge[111] ‖ Be[0001], Ge[110] ‖ Be[10$\bar{1}$0], and Ge[211] ‖ Be[11$\bar{2}$0]. X ray diffraction rocking-curve analysis and ion beam channeling show that the crystalline quality of these Ge films is poor compared to very good Ge films, such as Ge grown on Ge(111).

RHEED analysis of Ge films grown on thin Be buffers on Ge(111) indicate that Ge grows epitaxially at all temperatures investigated. However, for films grown at T ≤ 400 °C, faint transmission diffraction patterns are observed. These transmission patterns are characteristic of rough films. RHEED patterns of films grown at T = 500 °C indicate these films are smooth compared to those grown at lower temperature T. X ray diffraction analysis, RBS analysis, and ion beam channeling results are inconclusive for these samples due to the sample geometry. Specifically, the Be film is too thin to be characterized by any of these techniques. Also, because the Be film thickness is only ~50 Å, characteristics of the Ge overlayer cannot be resolved from those of the Ge substrate. Transmission electron microscopy (TEM) is currently in progress to characterize these samples.

Results for Be films grown on Ge(111) and Ge films grown on 500 Å Be buffer layers on Si(111) are shown in Table 2 and Table 3.

In conclusion, our results show that very high quality Be thin films may be grown on Ge(111). We have demonstrated the effects of substrate temperature and substrate quality on the quality of the Be film and postulated some explanations for these effects. In addition, we have shown epitaxial growth of Ge on Be(0001). This is a significant first step toward Be/Ge heterostructures. Such structures may be potentially useful in the areas of x ray optics and electronics.

Table 2. X-ray diffraction and ion beam channeling results for Be on Ge buffer layers.

Substrate	T (°C)	Rocking Curve FWHM	χ_{min}
Si(111)	200	.50	.53
Si(111)	300	.38	.52
Si(111)	400	.35	.45
Ge(111)	200	.30	.25
Ge(111)	300	.19	.18
Ge(111)	400	.20	.39

Table 3. X-ray diffraction and ion beam channeling results for Ge on 500 Å Be buffer layers.

Substrate	T (°C)	Rocking Curve FWHM	χ_{min}
Si(111)	300	polycrystalline	polycrystalline
Si(111)	425	.60	.64

Non-specular X ray Scattering from Multilayer X ray Mirrors

We have observed resonant non-specular x ray scattering effects in Si/Mo multilayers and have described the experimental techniques and results in previous reports. Using a simple analysis of the data, based on recent theories of x ray scattering from periodic multilayers, we previously used our measurements to determine that correlated roughness was present in these multilayers for spatial periods $l > 200$ Å. In order to extract more structural information, a specific model must be chosen. The model must include the power spectra of the interfaces and describe how the roughness is propagated through the stack. In collaboration with Daniel Stearns at Lawrence Livermore Laboratory, this type of detailed analysis of the data for a series of Si/Mo multilayer (sputter-deposited at 3, 6, 9, and 12 mtorr Ar pressure) has now been completed. Using a growth model developed by Stearns where the growth is parameterized in terms of a relaxation parameter ν describing the damping of features with increasing film thickness and Ω representing the volume of a growth unit. The results are the power spectral density (PSD) of the roughness as a function of spatial frequency and number of layers and a correlation number as a function of spatial frequency. The results show that roughness with $l > 1000$ Å is correlated over hundreds of bilayers, but the correlation number drops rapidly with increasing spatial frequency. For $l < 100$ Å the roughness is effectively uncorrelated (correlation number < 2 bilayers).

Results

Figure 1 shows a measured scatter curve through the fifth order Bragg peak for a Si/Mo multilayer with a period of 124.7 Å and the calculated fits. In this figure the scattering angle is the angle of the detector with respect to normal. The peak positions observed in this scatter curve correspond to $l > 200$ Å. Calculations were performed with and without the roughness of the superpolished substrate ($\sigma \approx 1$ Å) included in the model. In this case, the substrate roughness had little effect. For samples made on float glass ($\sigma \approx 5$ Å), the substrate roughness affected the non-specular intensity for peaks corresponding to approximately $l > 1000$ Å.

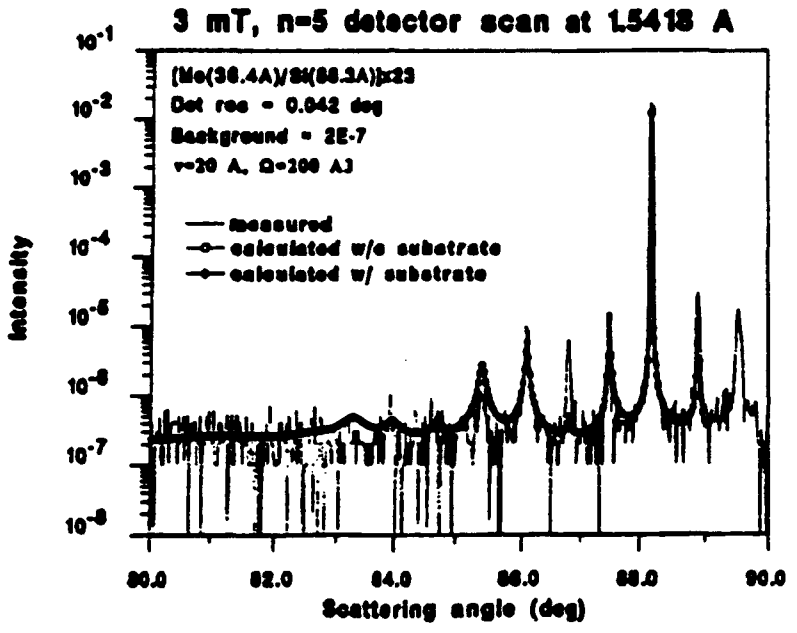

Figure 1. A measured scatter curve through the third order Bragg peak for a Si/Mo multilayer with a period of 124.7 Å and the calculated fits. The scattering angle is the position of the detector from normal.

Good fits were obtained for the 3 and 6 mtorr samples. Although the roughness increased from 3 to 6 mtorr, it was at 9 mtorr that the multilayer structure became severely distorted by columnar-like growth. The fits to the 9 mtorr are much more uncertain because of the additional peak broadening, evident in the specular data, that is not correctly accounted for by the model. The results of the fitting are shown in Table 4. The variation of the parameters with Ar pressure is consistent with a simple interpretation. Recall that ν characterizes the range of adatoms on the surface and Ω characterizes the average cluster size. At higher pressure, the sputtered atoms undergo more frequent collisions on the way to the growing film, and therefore arrive with lower energy. Thus, at higher pressure, both ν and Ω might be expected to decrease due to reduced surface mobility, as is seen in Table 4.

In summary, we have made non-specular x ray scattering measurements on Si/Mo multilayers using a low-angle diffractometer and Cu K_α radiation. These data have been analyzed quantitatively, using a theory of x ray scattering from non-ideal multilayers and a simple model of thin film growth. The analysis determined the (frequency dependent) PSD of the interfaces, and values for parameters that describe the film growth. The variation of these parameters with pressure reflects the changing mobility of the depositing atoms. We now have developed this technique to the point that it can be used to

determine not only the magnitude of the roughness but its origin. This information is invaluable in improving both the substrate surface roughness and the intrinsic multilayer roughness.

Table 4. Values for the average volume of the growth unit Ω, and the relaxation parameter ν, as determined from fits to the scatter curves.

Ar Pressure (mtorr)	ν (Å)	Ω (Å^3)
3	20	200
6	10	100
9	10	10

FUNDAMENTAL PHYSICS OF MBE HETEROSTRUCTURES

H.M. Gibbs

PUBLICATIONS AND PRESENTATIONS

1. D. Boggavarapu, R. Jin, J.W. Grantham, Y. Hu, F. Brown de Colstoun, C.W. Lowry, G. Khitrova, S.W. Koch, M. Sargent III, H.M. Gibbs and W. Chow, "Instabilities of a microcavity laser with weak injected signal," Opt. Lett. 18, 1846 (1993).

2. C.W. Lowry, F. Brown de Colstoun, A.E. Paul, G. Khitrova, H.M. Gibbs, J.W. Grantham, R. Jin, D. Boggavarapu, S.W. Koch, M. Sargent III, T.M. Brennan and B.E. Hammons, "Acceleration of coherent transfer of energy by stimulated emission and absorption," Phys. Rev. Lett. 71, 1534 (1993).

3. C.W. Lowry, F. Brown de Colstoun, G. Khitrova, H.M. Gibbs, A.W. Paul, S.W. Koch, T.M. Brennan and B.E. Hammons, "Asymmetric gain and intermodal asymmetry transfer in a vertical-cavity surface-emitting laser," QTuK5, QELS '93.

4. F. Brown de Colstoun, C.W. Lowry, G. Khitrova, H.M. Gibbs, A.E. Paul, S.W. Koch, T.M. Brennan and B.E. Hammons, "Asymmetric gain in a vertical-cavity surface-emitting laser," Topical Meeting on Quantum Optoelectronics.

5. H.M. Gibbs, "Acceleration of coherent transfer of energy by stimulated emission and Absorption in a vertical-cavity surface-emitting laser," Laser Optics '93, St. Petersburg, June 21-25, 1993, plenary talk; and C.W. Lowry, G. Khitrova, F. Brown de Colstoun, A.E. Paul, H.M. Gibbs, J.W. Grantham, R. Jin, D. Boggavarapu, S.W. Koch, M. Sargent III, T.M. Brennan and B.E. Hammons, "Power broadening of coherent energy transfer in semiconductor gain media," Laser Optics '93, St. Petersburg, June 21-25, 1993, proceedings paper.

6. H.M. Gibbs, G. Khitrova, C.W. Lowry, D. Boggavarapu, F. Brown de Colstoun, R. Jin, J.W. Grantham, A.E. Paul, Y. Hu, S.W. Koch, M. Sargent III, T.M. Brennan and B.E. Hammons, "VCSELs with injection: instabilities and local gain modification," CSNO '93, invited talk; and C.W. Lowry, H.M. Gibbs, G. Khitrova, D. Boggavarapu, F. Brown de Colstoun, R. Jin, J.W. Grantham, A.E. Paul, Y. Hu, S.W. Koch, M. Sargent, T.M. Brennan and B.E. Hammons, "Injection induced instabilities and local gain modification in VCSELs," CSNO '93, proceedings paper.

7. G. Khitrova, C.W. Lowry, F. Brown de Colstoun, A.E. Paul, H.M. Gibbs, J.W. Grantham, R. Jin, D. Boggavarapu, S.W. Koch, M. Sargent III, T.M. Brennan and B.E. Hammons, "Acceleration of coherent transfer of energy by stimulated emission and absorption," International Conference on Nonlinear Optics and Physical Applications (ICNOPA '93), Nanjing, PRC, Sept. 6-10, invited talk.

8. H.M. Gibbs, "Nonlinear optics of semiconductor heterostructures," International Topical Conference on Research Trends in Nonlinear and Quantum Optics, La Jolla, Nov. 22-24, 1993, invited talk.

9. S.G. Lee, R. Jin, B.P. McGinnis, J. Yumoto, G. Khitrova, H.M. Gibbs, S.W. Koch and N. Peyghambarian, "Subpicosecond switching in a current injected GaAs/AlGaAs multiple-quantum-well nonlinear directional coupler," submitted to Appl. Phys. Lett.

10. N. Peyghambarian, H.M. Gibbs, G. Khitrova, S.W. Koch and E.M. Wright, "Propagation-induced escape from adiabatic following in a semiconductor," Optics and Photonics News, p. 16, Dec. 1992, "Optics in 1992."

11. N. Peyghambarian, B.P. McGinnis, P. Harten, A. Knorr, S.G. Lee, R. Jin, E. Wright, G. Khitrova, H.M. Gibbs and S.W. Koch, "Femtosecond pulse propagation effects in semiconductors," QTuB5, QELS '93.

SCIENTIFIC PERSONNEL

Curt Lowry, Graduate Student
Deepak Boggavarapu, Graduate Student
Ruxiang Jin, Research Assistant Professor
Hyatt Gibbs, Professor

DEGREES AWARDED

Curt Lowry, Ph.D., May 1993
Deepak Boggavarapu, Ph.D., Aug. 1993

RESEARCH FINDINGS

Route-to-Injection Locking[1]

We injected a stable coherent beam into a vertical-cavity surface-emitting laser (VCSEL) and studied the route-to-injection locking as a function of the injected power. Pushing or pulling of the original lasing was seen, accompanied by the appearance of new frequencies. The behavior depends upon the sign of the detuning of the injection from the original lasing. We have compared these results with a semiconductor theory of injection locking and have obtained excellent agreement. This understanding and ability to accurately model can be very useful in injection-locking arrays of VCSELs.

By comparing the locking range for positive and negative detuning Δ, it is possible to estimate the alpha parameter α. Figure 1 shows the experimental data points for reciprocal locking power as a function of frequency detuning, from which we deduce an α between 1.4 and 2.6. This covers our previously measured value 2.0 ± 0.5 and the plasma-theory computed value of 2.27.[1]

Local Gain Asymmetry and the Generation of New Frequencies[2-8]

When a stable coherent beam is injected into a VCSEL that is lasing just above threshold, we see a modification of the emission spectrum as the injected power is increased. The emission is enhanced below the injection frequency and reduced above. These few-GHz modifications that occur for few-microwatt injections arise from coherent energy transfer involving spatial gratings written by the pump and probe, which involve the total carrier density.

When the injection is mid-range (10 μW to 40 μW) and tuned close to the high-frequency side of the VCSEL lasing [and the VCSEL lasing is strong and narrow ($\leq$ 1.5 GHz)], a new frequency is generated at about 5 GHz to the long wavelength side of the injection. As the injection power is increased, the new frequency shifts to longer wavelengths by as much as 25 GHz, linearly *proportional to the intracavity power at the injection frequency*; see Fig. 2. Both the new frequency and the injection can have relaxation oscillation sidebands, showing that the new frequency is not a relaxation oscillation sideband. The distorted dispersive shape of the local gain modification and the linear dependence of the

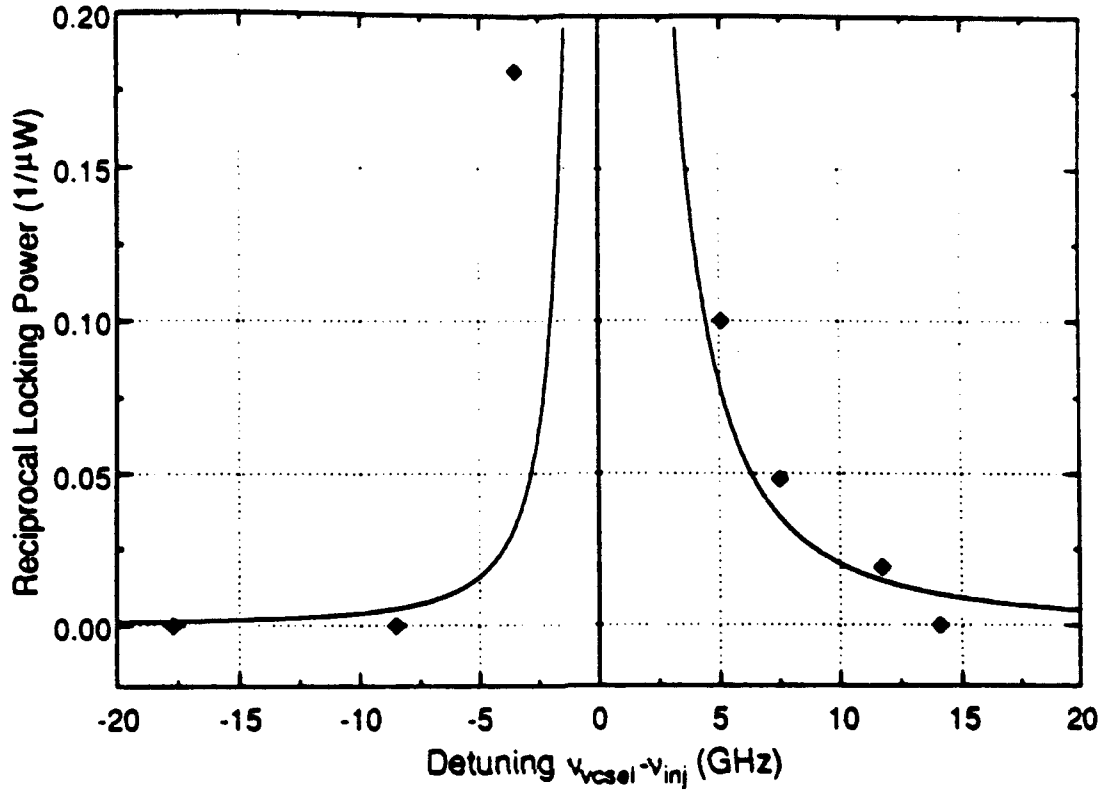

Figure 1. Reciprocal of the injection power level needed to frequency lock the VCSEL as a function of detuning. The solid curve shows the functional form of the locking range equation as asymmetry assuming $\alpha = 2.0$.

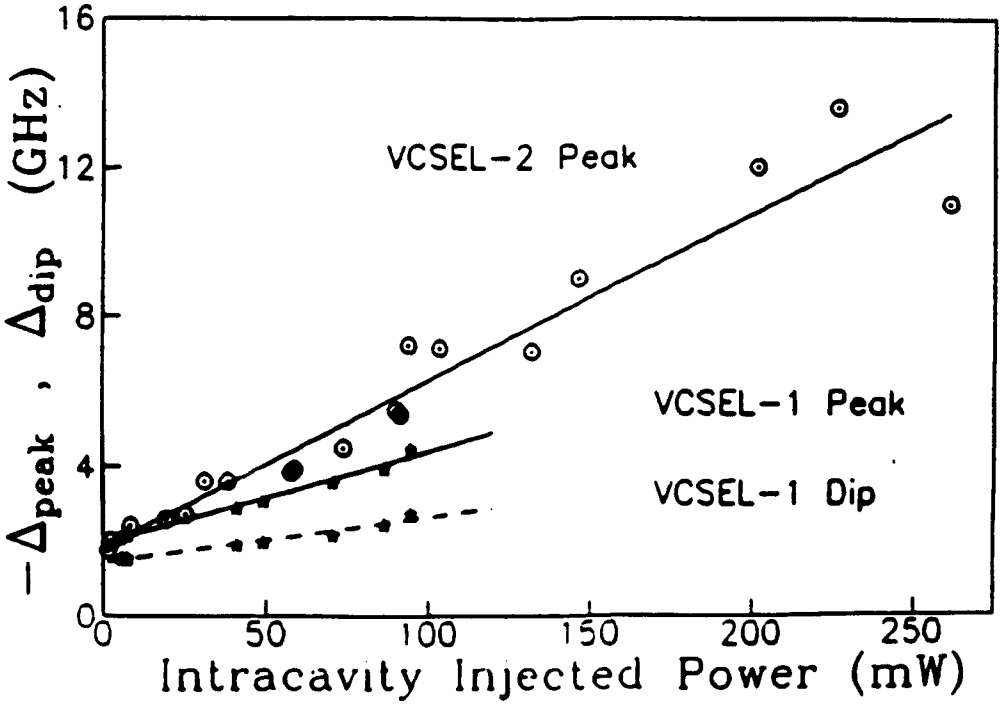

Figure 2. Acceleration of coherent transfer of energy by stimulated emission and absorption. Absolute detunings, $|\Delta_{peak,dip}| = |\nu_{peak,dip} - \nu_{inj}|$, from two series of spectra like that in (a), follow calculations of the gain peak (solid) and dip (dashed); from Ref. 2

new gain peak upon intracavity injected power are both explained quantitatively by a semiconductor theory of coherent energy transfer. A full understanding of strong injection effects on the semiconductor gain curve can help in the understanding of VCSEL instabilities.

The VCSEL lases in two nearly degenerate cross-linearly polarized modes, one of which is stronger by a factor of about 100 for lasing well above threshold. A weak injection may switch the polarization of the VCSEL lasing, exchanging the roles of the strong and weak modes. Local gain changes induced in one mode's spectrum appear in the VCSEL's other polarized mode (but not in higher-order modes). The Rayleigh-gain spatial grating written in one polarization is also seen in the other polarization, which has a different frequency but the same wavelength and wavevector in the material; see Fig. 3.[2]

Subpicosecond Nonlinear Directional Coupler[9]

We have collaborated with Peyghambarian's group to demonstrate subpicosecond switching and recovery of the transmission of the nonlinear directional coupler with current injection, which we fabricated previously with the help of Boeing Aerospace. The previous performance of this NLDC with 10-ps pulses was very little better than that of a passive NLDC. The much better performance with 100-fs pulses occurs at the no-gain/no-loss point (chemical potential), as shown earlier in a single waveguide laser amplifier by Hultgren and Ippen. The physics of the subpicosecond recovery is still controversial, and we and others continue to unravel it.

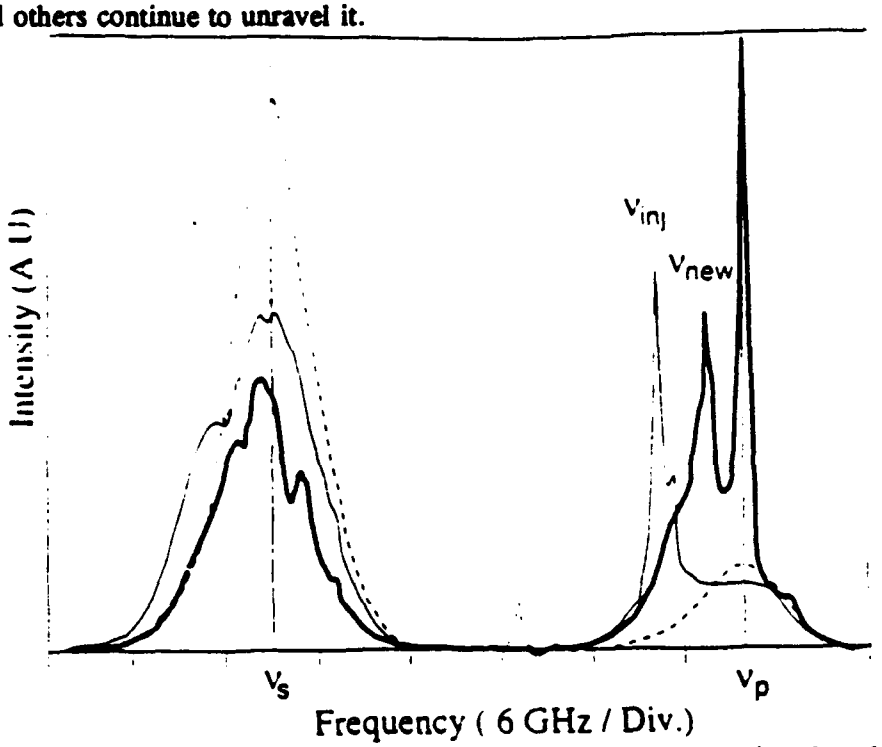

Figure 3. The no-injection VCSEL spectrum (dashed) has an s-polarized mode and a p-polarized mode which are both modified by the p-polarized injection (12 μW intracavity power) at ν_{inj} (thin line). A 20 μW intracavity injection at ν_p modifies both modes and produces a 10 μW new lasing line at ν_{new} which also modifies both modes.

MBE GROWTH OF NOVEL SEMICONDUCTOR HETEROSTRUCTURES

G. Khitrova

PUBLICATIONS AND PRESENTATIONS

1. F. Brown de Colstoun, A.V. Fedorov, G. Khitrova, T.R. Nelson, C.W. Lowry, H.M. Gibbs, T.M. Brennan and B.G. Hammons, "Gaussian-beam-induced vortices in vertical-cavity surface-emitting lasers," submitted to IQEC '94.

2. G. Khitrova, F. Brown de Colstoun, C.W. Lowry, E.M. Wright, H.M. Gibbs, T.M. Brennan and B.E. Hammons, "Spatial patterns in semiconductor lasers," LEOS '93, invited talk.

3. G. Khitrova, "Spatial patterns in nonlinear optics," International Symposium on Polymers POLYMEX-93, Nov. 1-5, 1993, Cancun, Mexico, invited talk.

4. G. Khitrova, H.M. Gibbs, Y. Kawamura, H. Iwamura, T. Ikegami, J.E. Sipe and L. Ming, "Spatial solitons in a self-focusing semiconductor gain medium," Phys. Rev. Lett. **70**, 920-923 (1993).

5. G. Khitrova, H.M. Gibbs, J.W. Grantham, M. Liang, J. Xu, J.F. Valley, C.W. Lowry, F. Brown de Colstoun, Y. Kawamura, H. Iwamura and T. Ikegami, "Spatial solitary waves, solitons, and vortices," Workshop on Computer Simulations in Nonlinear Optics (CSNO '93), June 26 - July 4, Volga Laser Tour, invited talk; and F. Brown de Colstoun, G. Khitrova, H.M. Gibbs, J.W. Grantham, M. Liang, J. Xu, J.F. Valley, C.W. Lowry, Y. Kawamura, H. Iwamura and T. Ikegami, "Spatial solitary waves, solitons, and vortices," proceedings paper.

6. J.W. Grantham, G. Khitrova, H.M. Gibbs, J.F. Valley and J. Xu, "Bifurcations of optical transverse solitary waves," *Transverse Patterns in Nonlinear Optics*, SPIE **1840**, 25-42 (1991, printed in 1993).

7. R. Jin, M. Liang, G. Khitrova, H.M. Gibbs and N. Peyghambarian, "Compression of bright optical pulses by dark solitons," Opt. Lett. **18**, 494-6 (1993).

8. R. Jin, D. Boggavarapu, M. Sargent III, P. Meystre, H.M. Gibbs and G. Khitrova, "Photon-number correlations in a microcavity laser," APS March Meeting.

9. H.M. Gibbs, R. Jin, D. Boggavarapu, M. Sargent III, P. Meystre and G. Khitrova, "Photon-number correlations near the threshold of microcavity lasers," ICNOPA '93, invited talk.

10. R. Jin, D. Boggavarapu, M. Sargent III, P. Meystre, H.M. Gibbs and G. Khitrova, "Photon-number correlations near the threshold of a microcavity laser," submitted to Phys. Rev. A.

11. M.F. Krol, T. Ohtsuki, G. Khitrova, B.N. Boncek, B.P. McGinnis, H.M. Gibbs and N. Peyghambarian, "All-optical high contrast GaAlInAs multiple quantum well asymmetric reflection modulator at 1.3-μm," Appl. Phys. Lett. **62**, 1550 (1993).

12. N. Peyghambarian, T. Ohtsuki, G. Khitrova, H.M. Gibbs, B.P. McGinnis, M.F. Krol and R.K. Boncek, "30 dB contrast GaAlInAs multiple quantum well asymmetric reflection modulator at 1.3 μm," Optics and Photonics News, p. 19, Dec. 1993. "Optics in 1993."

13. T. Ohtsuki, M.F. Krol, G. Khitrova, R. Jin, R.K. Boncek, B.P. McGinnis, H.M. Gibbs and N. Peyghambarian, "All-optical asymmetric Fabry-Perot reflection modulators," Int. J. Nonlinear Optical Physics 2 (1993).

SCIENTIFIC PERSONNEL

Galina Khitrova, Assistant Professor
Francois Brown de Colstoun, Graduate Student
Tom Nelson, Graduate Student
Eric Lindmark, Graduate Student
Alexander Fedorov, Visiting Scientist

RESEARCH FINDINGS

Gaussian-Beam-Induced Vortices in Vertical-Cavity Surface-Emitting Lasers[1-3]

We have triggered transverse pattern modifications by injecting a CW monochromatic (10 MHz) beam into a vertical-cavity surface-emitting laser (VCSEL). The injected Gaussian beam has a frequency close to that of the natural TEM_{00} mode of the VCSEL (Fig. 1). The spot of the injection is not superimposed with the original lasing spot (Fig. 2). However, it is close enough to lock the TEM_{00} mode, as seen in the interferogram of Fig. 3. As a result, we observe a system of two Gaussian beams locked in frequency and in phase, propagating on parallel axes, and with waists of different size and location. The interferogram of Fig. 3 shows two vortices of opposite topological charges located on both sides of the system of two Gaussian beams.

Rosanov has shown theoretically [Optika i Spektroskopiya 75, 861 (1993)] that if such a system had the two beams propagating along the same axis, a series of vortices would appear, with their trajectories along concentric rims normal to the axis of propagation. These vortices do not display the phase singularity behavior in the plane normal to the axis of propagation and cannot be observed interferometrically. However, when the beams' axes are not collinear, vortices appear with their trajectories along lines oriented in the same direction as the axes, and thus, can be observed as phase singularities in the plane normal to the axes of propagation. In our experiment, the image plane coincided with the focal plane of the injected beam, at the VCSEL/air plane. In this plane, in a bipolar coordinate system (r_1, r_2) with poles coinciding with axes of the beams, the locations of vortices are given by the following formulas:

$$r_1^2 = 2\left[1 + \left[m + \frac{1}{2}\right]\frac{\lambda}{D}\right]\left[D^2 + \pi^2\frac{w_1^4}{\lambda^2}\right], \quad m = 0, \pm 1, \pm 2, \ldots$$

$$r_2^2 = w_2^2\left[\frac{r_1}{w_1^2 + \lambda^2 D^2/\pi^2 w_1^2} - \ell n\frac{A_1}{A_2}\right],$$

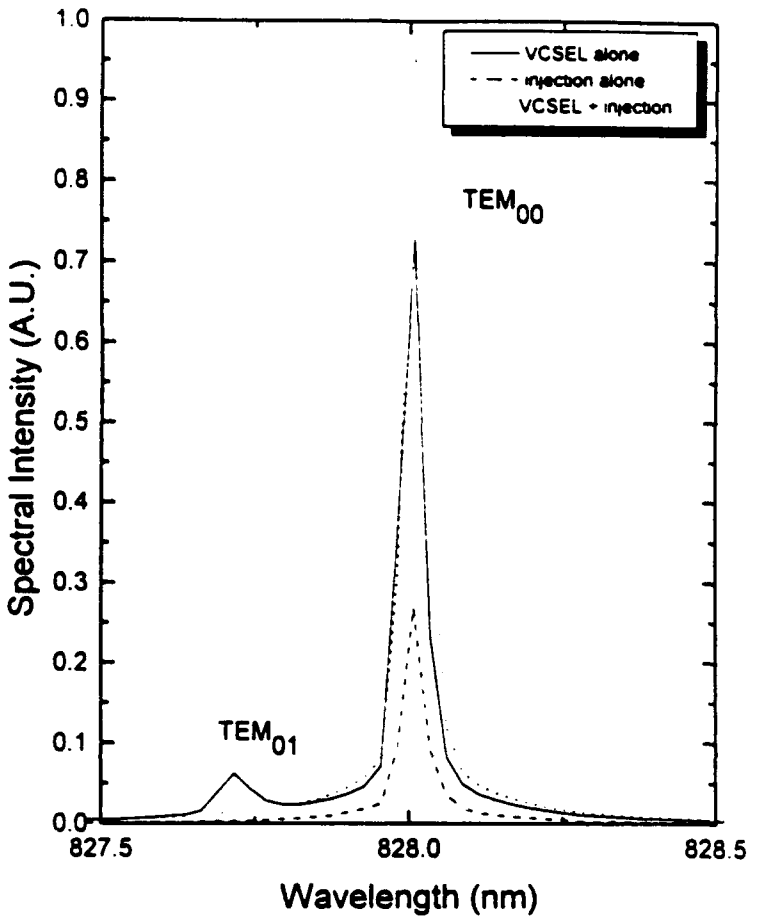

Figure 1. Injecting (dashed curve) at the frequency of the TEM_{00} mode modifies the original lasing spectrum (solid curve), and locks the laser in a pure TEM_{00} mode (dotted curve).

where index 1 stands for the laser beam, and index 2 stands for the injected beam. D is the distance between focal planes of the two beams; w_j are half-waists of the beams; A_j are beam amplitudes; and λ is the wavelength.

The pair of vortices observed in the experiment corresponds to the order m = -15. A neighboring pair of vortices should be located outward at a distance of more than 5 μm from the observed vortices. In our experimental setup, it is currently out of observation. The distance between the beams' axes is not a parameter in the above formulas. Hence, bringing the beams closer increases the distance between the vortices, and vice versa. This dependence was clearly confirmed in the experiment. Likewise, r_2 linearly depends on w_2. When w_2 increases, r_2 increases also, separating the two vortices further. These changes in positions of the vortices also were clearly seen in the experiment.

We conclude that our VCSELs do not emit vortices. The vortices observed with injection are an interference between the VCSEL emission and the injection. Stationary fringes between VCSEL and injection-frequency reference beams cannot be seen without injection locking. Furthermore, efficient locking requires focusing of the injection onto the VCSEL. For these reasons, it was nontrivial to conclude that the vortices arise from the interference of two beams (VCSEL and injection) with waists in the same plane, rather than from the VCSEL emission itself. This is another example of the appearance of vortices in linear optics, just as in optical testing experiments.

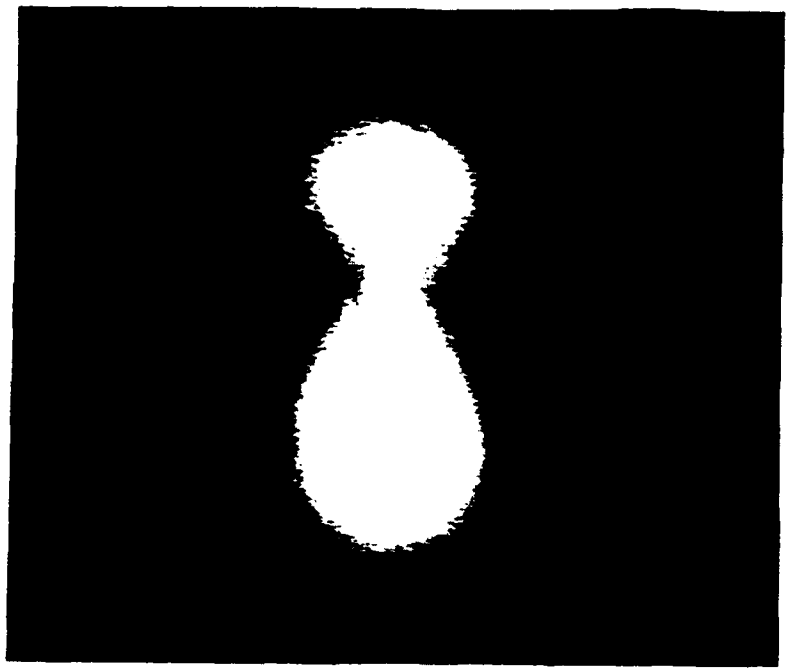

Figure 2. The original lasing spot at the output mirror of the VCSEL is the one on top of the pattern. The injection has been positioned underneath. The injection is close enough to lock the VCSEL lasing in frequency and in phase.

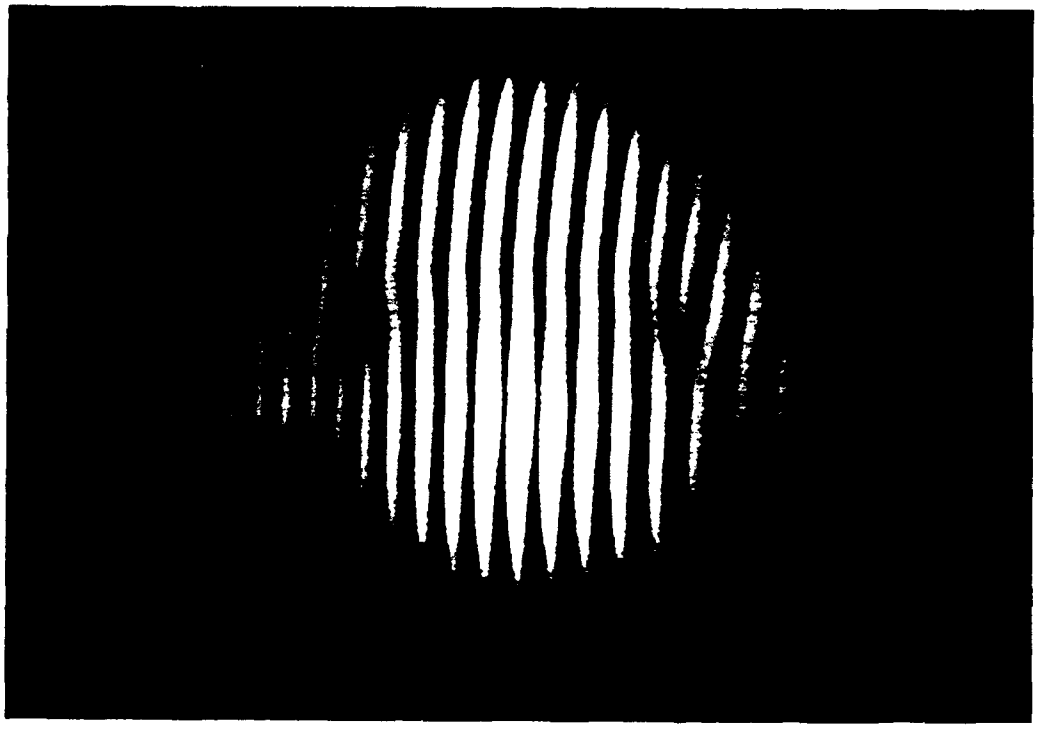

Figure 3. An interferogram of the intensity pattern of Fig. 2 shows two vortices of opposite topological charge. These vortices move up and outward as the waist of the injection is increased or as the injection is brought closer to the original lasing spot of the VCSEL.

Spatial Solitons in a Self-Focusing Semiconductor Gain Medium[4]

A beam propagating in a planar waveguide exhibits the characteristics of both a fundamental soliton (little change in waist of a 5-μm beam; diffraction is compensated by self-focusing nonlinear refraction) and a second-order soliton (10-μm beam focuses to 3 μm with side peaks). These one-dimensional spatial solitons are quite stable; bifurcations of transverse solitary waves are not seen, in sharp contrast with the case for two transverse dimensions.[5,6] Plasma-theory planar-wave beam-propagation computations agree well with the data and resemble Kerr-medium solitons quite closely.

Compression of Bright Optical Pulses

This is a theoretical prediction of the compression of bright optical pulses by copropagation with a dark temporal soliton, an extension of ideas from our earlier paper on induced (spatial) focusing in a semiconductor defocusing medium.[7]

Photon-Number Correlations Near the Threshold of Microcavity Lasers[8-10]

We made the first second-order correlation measurement of a VCSEL and found that the peak of the Fano-Mandel parameter $K = [\langle n^2\rangle - \langle n\rangle^2 - \langle n\rangle]/\langle n\rangle = \langle n\rangle[g^{(2)}(0) - 1]$ occurs at the same pump intensity that the derivative of the output intensity becomes discontinuous, for our $\beta = 0.0065$ for the fraction of spontaneous emission going into the lasing mode. As $\beta \to 1$, the discontinuity in output power vanishes; some people call this a thresholdless laser. We suggest that since the low-pump emission is simply spontaneous emission, it is better described as LED rather than laser emission. Using two-level-atom photon statistics with GaAs parameters, we show that the intensity fluctuations of the field, quantified by K, still exhibit a maximum because of the transition from spontaneous to stimulated emission. The transition of $g^{(2)}(0)$ from 2 to 1 at lasing threshold becomes softer and softer as $\beta \to 1$. Therefore, *we conclude that there is no thresholdless laser.*

OPTICAL NONLINEARITIES IN LOW-DIMENSIONAL SEMICONDUCTOR STRUCTURES

S.W. Koch and N. Peyghambarian

PUBLICATIONS AND PRESENTATIONS

N. Peyghambarian, S.W. Koch and A. Mysyrowicz, *Introduction to Semiconductor Optics* (Prentice Hall, Englewood Cliffs, New Jersey, 1993).

H. Haug and S.W. Koch, *Quantum Theory of the Optical and Electronic Properties of Semiconductors*, Second Edition (World Scientific, Singapore, 1993).

L. Banyai and S.W. Koch, *Semiconductor Quantum Dots* (World Scientific, Singapore, 1993).

N. Peyghambarian, E. Hanamura, S.W. Koch, Y. Masumoto and E.M. Wright, "Optical characterization and applications of semiconductor quantum dots," in A.S. Edelstein and H. Hahn, eds. *Nanostructured Materials: Synthesis, Characterization, and Uses* (Adam Hilger, 1993).

K. Kang, A.D. Kepner, S.V. Gaponenko, S.W. Koch, Y.Z. Hu and N. Peyghambarian, "Confinement-enhanced biexciton binding energy in semiconductor quantum dots," Phys. Rev. B **48**, 15449 (1993).

K.I. Kang, B. McGinnis, Sandalphon, Y.Z. Hu, S.W. Koch, N. Peyghambarian, A. Mysyrowicz, L.C. Liu and S.H. Risbud, "Investigation of confinement-induced valence band mixing in CdS quantum dots by two-photon spectroscopy," Phys. Rev. B **45**, 3465 (1992).

V. Esch, K. Kang, B. Fluegel, Y.Z. Hu, G. Khitrova, H.M. Gibbs, S.W. Koch and N. Peyghambarian, "Optical properties of CdTe and CdS quantum dots in glass," Int. J. Nonlinear Opt. Phys. **1**, 25 (1992).

S.W. Koch, Y.Z. Hu, B. Fluegel and N. Peyghambarian, "Coulomb effects and optical properties of semiconductor quantum dots," J. Cryst. Growth **117**, 592 (1992).

S.W. Koch, A. Knorr, R. Binder and M. Lindberg, "Microscopic theory of Rabi flopping, photon echo, and resonant pulse propagation in semiconductors," Phys. Status Solidi B **173**, 177 (1992).

W.S. Fu, J.S. Harris, R. Binder, S.W. Koch, J.F. Klem and G.R. Olbright, "Nonlinear optical properties and ultrafast response of GaAs/AlAs type-II quantum wells," IEEE J. Quantum Electron. **28**, 2404 (1992).

A. Knorr, R. Binder, M. Lindberg and S.W. Koch, "Theoretical study of resonant ultrashort pulse propagation in semiconductors," Phys. Rev. A **46**, 7179 (1992).

R. Jin, K. Okada, G. Khitrova, H.M. Gibbs, M. Pereira, S.W. Koch and N. Peyghambarian, "Optical nonlinearities in strained layer InGaAs/GaAs multiple quantum wells," Appl. Phys. Lett. **61**, 1745 (1992).

S.W. Koch, D.C. Scott and R. Binder, "Optical dephasing and acoustic plasmon undamping in highly excited semiconductors," Opt. & Phot. News **3** (12), 14 (1992).

N. Peyghambarian, H.M. Gibbs, G. Khitrova, S.W. Koch and E.M. Wright, "Propagation induced escape from adiabatic following in a semiconductor," Opt. & Phot. News **3** (12), 16 (1992).

S.W. Koch, Y.Z. Hu and R. Binder, "Photon echo and exchange effects in quantum-confined semiconductors," Physica B 189, 176 (1993).

K. ElSayed, R. Binder, D.C. Scott and S.W. Koch, "Undamping of acoustic plasmons in nonequilibrium plasmas," Phys. Rev. B 47, 10210 (1993).

Y.Z. Hu, R. Binder and S.W. Koch, "Photon echo and valence-band mixing in semiconductor quantum wells," Phys. Rev. B 47, 15679 (1993).

M. Bonitz, R. Binder and S.W. Koch, "Carrier-acoustic plasmon instability in semiconductor quantum wires," Phys. Rev. Lett. 70, 3788 (1993).

S.W. Koch, "Theory of linear and nonlinear optical properties of semiconductor quantum dots," 182nd Meeting of the Electrochemical Society, Toronto, Canada, Oct. 11-16, 1992 (invited).

N. Peyghambarian, "Recent advances in nonlinear quantum dots in glass," The Annual Meeting of the Optical Society of America, Toronto, Canada, Oct. 3-8, 1993 (invited).

S.W. Koch, "Theory of semiconductor quantum dots," Conference on II-VI Semiconductors, Japan, 1992 (invited).

N. Peyghambarian, "The application of nonlinear optical materials based on ultrafine particles," International Workshop on Ultrafine Particles in Glass, Nov. 10-11, 1992, Osaka, Japan (keynote address).

N. Peyghambarian, "Quantum confinement and applications," Conference on Nonlinear and Quantum Optics, Rio de Janeiro, Brazil, October 19-23, 1992 (invited).

S.W. Koch, Y.Z. Hu, B. Fluegel and N. Peyghambarian, "Excitons, biexcitons, and optical nonlinearities in semiconductor quantum dots," Inst. Phys. Conf. Ser. No. 123 (1992) p. 139, Proc. Int. Conf. on Optics of Excitons in Confined Systems, Giardini Naxos, Italy (invited).

K. Kang, B.P. McGinnis, Sandalphon, Y.Z. Hu, S.W. Koch, N. Peyghambarian, A. Mysyrowicz, L.C. Liu and S.R. Risbud, "Two-photon spectroscopy of CdS quantum dots," Inst. Phys. Conf. Ser. No. 123 (1992) p. 245, Proc. Int. Conf. on Optics of Excitons in Confined Systems, Giardini Naxos, Italy (invited).

SCIENTIFIC PERSONNEL

Rudolf Binder
Yuan Hu
Brian McGinnis
Tomoko Ohtsuki

RESEARCH FINDINGS

In this project we proposed to perform theoretical and experimental studies of the linear and nonlinear optical properties of low-dimensional semiconductor structures, such as quantum dots, quantum wells, or more complicated heterostructures. Here we summarize our results.

CdS and CdSe Quantum Dot Research

Nonlinear absorption spectra of quantum-confined CdSe microcrystallites in glass were measured in a femtosecond pump-probe experiment at low temperatures. Simultaneous bleaching of the quantum-confined transitions and an induced absorption at higher energy were observed. Spectral hole burning was observed as the pump was tuned through the transition. The system was modeled as spherical crystallites with one or two electron-hole pairs interacting through the Coulomb potential. Our numerical matrix diagonalization method predicted results essentially similar to the experiment and attributed them to state filling of the one-pair states and generation of two-pair states.

The linear absorption spectra of three samples of CdS quantum dots in glass at 10 K are shown in Fig. 1. The spectrum labeled "bulk" refers to a glass with semiconductor microcrystallites large enough to retain the three-dimensional bulk properties. This spectrum is typical of a bulk CdS absorption spectrum with a sharp exciton and structureless Coulomb-enhanced continuum absorption at higher photon energies. The average crystallite size becomes smaller for lower heat-treatment temperatures. The spectra labeled "QD" refers to samples with small crystal sizes. The quantum-confinement effects are clearly observable in this sample. The absorption has shifted to higher energies, as expected for the confinement effect. Furthermore, discrete quantum-confined electron-hole-pair states appear in the "QD" sample.

An example of measured optical nonlinearities for quantum dots in glass is shown in Fig. 2. The absorption change for resonant excitation into the energetically lowest quantum-confined transition was measured. The top spectrum in Fig. 2 displays the linear absorption of a CdS-doped glass quantum-dot sample at T = 10 K. This spectrum has two peaks at energies of approximately 2.95 eV and 3.26 eV. The low-energy peak originates from the transition between the 1s-hole and 1s-electron states. The high-energy peak is due to the transition between the 1p-hole and 1p-electron states.

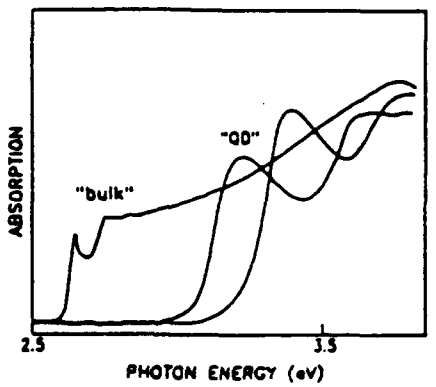

Figure 1. The linear absorption spectra at T = 10 K of CdS crystallites in glass. The two spectra labeled "QD" refer to two samples with small crystal sizes in the quantum-confinement regime. The "bulk" sample has large crystal sizes, exhibiting bulk CdS properties. (The samples were prepared by Liu and Risbud.)

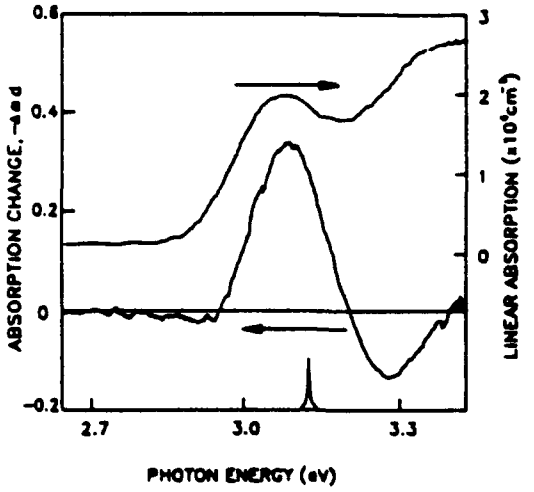

Figure 2. The top curve is the linear absorption spectrum of a sample of CdS quantum dots in glass. The bottom trace shows the energetic position of the pump pulse. The intermediate trace is the change in the linear absorption spectrum as a result of excitation by the pump pulse. d is the thickness of the sample. (The sample was prepared by Liu and Risbud.)

The narrow peak at the bottom of Fig. 2 displays the spectral position of the pump pulse. A broadband probe pulse detects the changes made in the absorption spectra as a result of excitation by the pump pulse. Probe absorption without previous excitation by the pump is equivalent to the generation of one electron-hole pair in the unexcited quantum dot. If, however, a pump photon has been absorbed previously, the probe beam generates a second electron-hole pair in the presence of the pump-generated pair.

The lower spectrum in Fig. 2 shows the measured changes in the absorption, $-\Delta\alpha d = d[\alpha_{probe}$ (without pump) - α_{probe} (with pump)]. In such a spectrum, a positive peak corresponds to bleaching and a negative peak indicates an induced absorption, i.e., an increase in the probe absorption as a consequence of the presence of the pump-generated electron-hole pair. The nonlinear spectrum in Fig. 2 shows a positive peak around the $1s_h$ - $1s_e$ transition, centered around the pump, and a negative peak on the high-energy side, centered around 3.178 eV. The bleaching of the $1s_h$ - $1s_e$ transition is the result of state filling. The generation of one electron-hole pair by the pump causes saturation of the one-pair transition (bleaching of the linear absorption peak).

The origin of the induced absorption feature (the negative peak in the lower spectrum of Fig. 2) is assigned to the generation of two-pair states in the quantum dot. The pairs are created by absorption of one pump and one probe photon. The theoretical analysis of the linear and third-order nonlinear optical properties has to include the one- and two-electron-hole-pair states. These investigations consistently lead to the conclusion that Coulomb effects are important even for the smallest quantum dots. Using numerical matrix diagonalization techniques, the energies and wave functions were obtained for the one- and two-pair ground states and for all the excited pair states. With these wave functions, the various dipole matrix elements were evaluated for transitions between the ground state and the one- and two-electron-hole-pair states. The changes in the absorption, $-\Delta\alpha d$, were then calculated, as shown in Fig. 3. Like the experiment, the theory also exhibits a decreasing absorption feature (bleaching) around the lowest quantum-confined transition and an increasing absorption feature on the high-energy side.

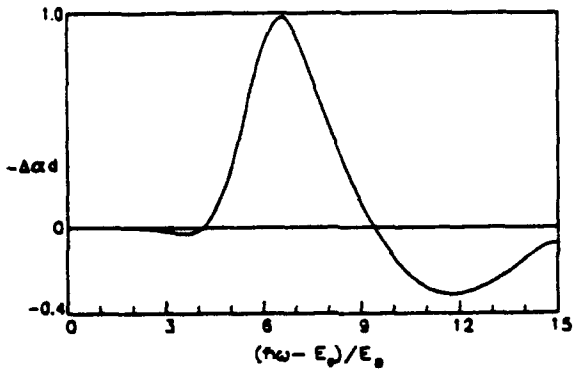

Figure 3. Computed absorption changes for a semiconductor quantum dot of radius R = a_B (where a_B is the exciton Bohr radius), assuming a pump and probe geometry, and pumping into the energetically lowest one-pair state.

Optical Nonlinearities of CdTe Quantum Dots[1,2,3]

We extended our quantum dot research to include microcrystallites of CdTe in glass matrices. CdTe has the largest Bohr radius of any semiconductor successfully grown as quantum dots in glass. Therefore, quantum-confinement effects can even be seen in larger dots.

To distinguish between intrinsic effects of photogenerated electron-hole pairs and effects of trapped charges, we measured the nonlinear absorption changes at early times using femtosecond laser pulses. Femtosecond pulses at ≈ 620 nm were generated in a colliding-pulse mode-locked dye laser cavity and were amplified by an 8.5 kHz copper vapor laser. Figure 4(a) shows the linear absorption spectrum of one of the CdTe quantum dot samples with average crystallite size of 36 Å. The S_A and S_B transitions in this figure correspond to two quantum-confined transitions that share the same electron levels. The measured absorption ($\delta\alpha L$) changes immediately after excitation inside the S_B line, and the pump spectral position is displayed in Fig. 4(b). The $\delta\alpha L$ spectrum consists of two features corresponding to bleaching of both S_A and S_B lines. The bleached S_B line has larger magnitude compared with the S_A bleaching, in spite of the fact that the linear S_A absorption is larger than S_B [see Fig. 4(a)]. These observations are reproduced by a simple model whose result is presented as the dashed line in the inset of Fig. 4. In this model, we take into account transitions between the ground state (no electron-hole pair) and the S_A and S_B one-pair states. In addition, we also include transitions to the excited two-pair states, which are energetically above the energy of twice the one-pair transitions. The size distribution of quantum dots is modeled as an inhomogeneous broadening of all the transitions. The qualitative agreement between Fig. 4(b) and the dashed spectrum of the inset shows that state filling of one-pair transitions is clearly responsible for the observed absorption saturation.

To further examine the state-filling effect, we tuned the pump pulse inside the S_A transition, as shown in Fig. 4(c). As expected, we see an S_A to S_B bleaching ratio that is not only larger than that of Fig. 4(b), but also larger than the linear S_A to S_B absorption coefficient ratio. Furthermore, an induced absorption feature is apparent on the high-energy side of the S_B bleaching. As shown by our model calculation in the inset of Fig. 4 (the solid curve), this induced absorption is the result of the two-electron-hole-pair transitions. The larger bleaching of S_A compared with S_B, and the induced absorption on the high-energy side in the spectrum shown by the solid line of the inset, are clearly similar to the experiment of Fig. 4(c).

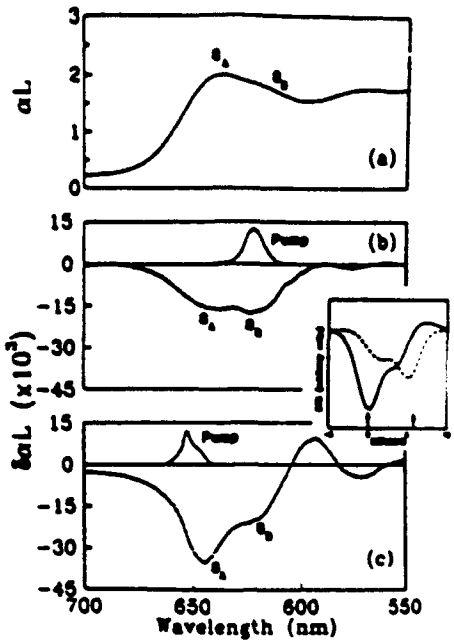

Figure 4. (a) Linear absorption of the CdTe quantum-dot sample at 15 K. (b) and (c) Measured absorption changes for pumping at ≈ 620 and ≈ 653 nm, respectively. The spectral location of the pumps are shown on the upper part of each figure. Inset: calculated absorption changes for the two pumping situations. The pump positions are displayed by arrows. The dashed spectrum (solid spectrum) is calculated for a detuning of 6 (zero), suitable for comparison with (b) [(c)]. (The sample was prepared by Liu and Risbud.)

We proposed the following scenario to explain the observed phenomena. The first photon creates an electron-hole pair inside the quantum dot. The pair creation may happen with or without the presence of charged impurities or trap states. Since the electron and hole interact via the attractive Coulomb potential, their wave functions deviate significantly from those of the strong-confinement approximation (no Coulomb interaction). There is strong evidence that the long-time behavior of the absorption changes are determined by carriers trapped at surface states (e.g., Cd^{2+} ions) or into localized states in the glass outside the quantum dot. The corresponding absorption changes result from the Coulomb interaction of the probe-generated electron-hole pairs with the trapped charges and state filling, which may become partial if a carrier leaves the dot. Therefore, state filling and Coulomb interaction are responsible for absorption changes at early times after excitation, and Coulomb effects are the only important mechanism for later times. Both photoinduced absorption changes and photoluminescence of traps have long-lasting components yielding evidence that long-lived nonlinear optical components are associated with traps.

Femtosecond Dynamics of Type II Quantum Wells

The many-body effects associated with a two-component plasma, i.e., electrons and holes, have been studied. In type-II quantum wells, on the other hand, the electrons are removed from the holes, and the dynamics of holes or electrons can be investigated separately. For example, when the GaAs layer thickness is less than 35 Å and AlAs layer thickness is greater than 16 Å, the lowest Γ-electron state of the GaAs well lies energetically above the X-minimum of the AlAs barrier, whereas the lowest energy hole state is still in the GaAs layer (see the inset of Fig. 5). As a result of such a band alignment, optical excitation of electron-hole pairs in the GaAs layer is followed by a spatial separation of the two plasma

components; electrons scatter from the Γ-state in GaAs to the X-state in AlAs. This allows the measurement of the dynamics of the hole relaxation in the GaAs layer where they are spatially separated from the electrons in the AlAs layer. We have made such measurements at T = 10 K using 130-fs laser pulses, tuned resonantly inside the heavy-hole exciton peak of a type-II quantum-well structure consisting of ≃28-Å-thick GaAs (10 monolayers) and ≃57-Å-thick AlAs (20 monolayers) layers.

Figure 5 displays the absorption spectra of the sample at various time delays between the pump and probe pulses together with the pump spectrum. A bleaching and blue shift of the absorption spectrum at both the light-hole and the heavy-hole excitons is clearly observed for the zero-ps time delay. Blocking of the conduction and heavy-hole states by the electrons, which have not yet left the GaAs layer, is responsible for this effect. In the 3-ps spectrum, the light-hole exciton blue shift is completely recovered, while the heavy hole is still bleached and shifted. This behavior is caused by the fact that the Γ-X electron scattering has already taken place and only the Γ-point heavy-hole phase-space filling is left. The relaxation (cooling) of the heavy holes contributes to the behavior of the 100-ps trace. Also, we observe a complete recovery of the light-hole exciton peak due to decreased screening of "cool" heavy holes. As the holes relax to the lowest energy states, the bleaching of the spectral region on the low-energy side of the heavy-hole exciton (see the region around $\lambda \simeq 670$ nm) is increased, while the bleaching of the high-energy side of the heavy-hole exciton (see the region around $\lambda \simeq 660$ nm) is recovered.

In our theoretical analysis of the many-body effects in the band-edge absorption spectra of highly excited type-I and type-II semiconductor quantum-well structures, we assumed perfect electron-hole charge separation, so that only the Γ-point holes contribute to phase-space filling of the GaAs exciton states. We numerically solved the interband polarization equation, including inhomogeneous broadening due to well-width fluctuations by averaging the spectra over a distribution of well thicknesses.

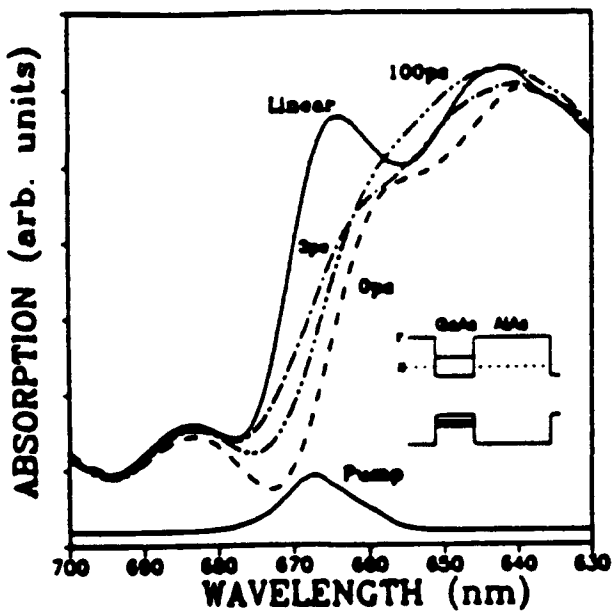

Figure 5. Absorption spectra at different time delays for resonant heavy-hole exciton pumping in a GaAs-AlAs type-II quantum well. The inset shows the energy level diagram for the sample.

Figure 6 shows computed quasi-equilibrium absorption spectra for different plasma densities. In the low-temperature spectra of Fig. 6(a), saturation and blue shifting of the HH exciton and a slight red shift of the LH exciton can be seen. For elevated plasma temperatures, Fig. 6(b) shows that the exciton blue shift is substantially reduced, since the holes' distributions involve more band states, substantially reducing Coulomb enhancement and Pauli blocking effects. The type-I results in Fig. 6(c) also show HH exciton saturation and blue shift, along with a blue shift of the LH exciton due to phase-space filling by the electrons.

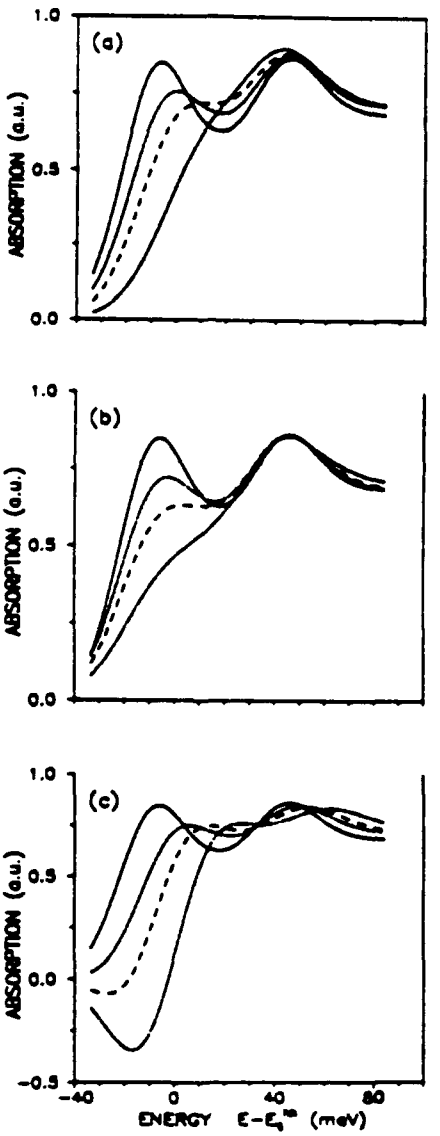

Figure 6. Computed absorption spectra for type-I and type-II quantum wells with GaAs well thickness of 30 Å. The spectra are for the plasma densities na_0^2 = 0.2 (short dashed), 0.4 (medium dashed), and 0.8 (long-short dashed). The linear spectra are shown as solid lines, and a_0 is the bulk-exciton Bohr radius. (a) Type-II, plasma temperature T = 30 K; (b) Type-II, T = 100 K; (c) Type-I, T = 30 K.

There is no gain in the type-II spectra, whereas clear regions of negative absorption develop in the type-I spectra. This absence of gain in moderately excited ideal type-II structures is a direct consequence of the spatial-electron and hole-plasma separation. The gain part of a type-I spectrum is replaced by a zero-absorption region in type-II structures where the quasi-chemical potential coincides with the onset of absorption for sufficiently high densities.

Photon Echo in Semiconductors

We began the theoretical study of the photon echo in semiconductors using the semiconductor Bloch equations. For the photon echo case, we assumed a configuration where the two exciting pulses are incident under an angle. We took the first pulse to be weak so that we could assume linear response. The strong second pulse was treated in all orders. The center frequencies of both pulses were at the 1s exciton resonance, assuming pulse separation of τ = 400 fs. Figure 7 shows that for the case of a weak first pulse, an almost instantaneous signal and no photon echo at +400 ps occurs. Our analytical calculations proved that this signal is due solely to the exchange correlation between the excited excitons. For higher pulse intensities, we see the gradual development of an echo signal, which coexists with the instantaneous signal for intermediate intensities.

To analyze the origin of this scenario, Fig. 8 plots the time dependence of the renormalized bandgap for the excitation conditions of Fig. 7. Comparing Figs. 7 and 8 reveals that the echo contribution in the time-resolved signal occurs as soon as the continuum states are shifted into resonance during the presence of the first pulse (bandgap shift below $-1E_R$ in Fig. 8). Consequently, direct continuum excitation is possible, which yields a photon echo signal at 400 fs because of the intrinsic inhomogeneous broadening of the electron-hole continuum states.

REFERENCES

1. Y.Z. Hu, S.W. Koch, M. Lindberg and N. Peyghambarian, Theoretical and experimental results on Coulomb effects in semiconductor quantum dots," Phys. Status Solidi B **159**, 249 (1990).

2. W.S. Fu, J.S. Harris, R. Binder, S.W. Koch, J.F. Klem and G.R. Olbright, "Nonlinear optical properties and ultrafast response of GaAs/AlAs type-II quantum wells," IEEE J. Quantum Electron. **28**, 2404 (1992).

3. A. Knorr, R. Binder, M. Lindberg and S.W. Koch, "Theoretical study of resonant ultrashort pulse propagation in semiconductors," Phys. Rev. A **46**, 7179 (1992).

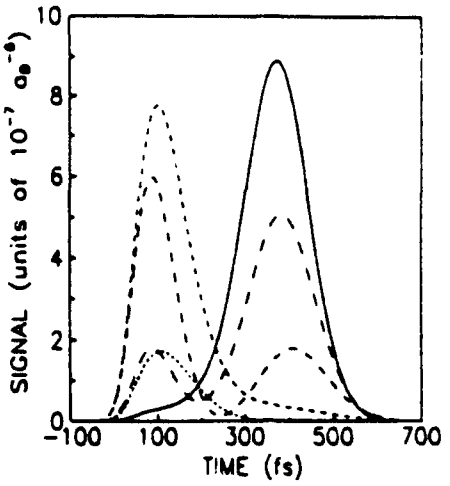

Figure 7. Time-resolved signal in the photon-echo direction for increasing strength of the first pulse, E_1. Excitation occurs at the exciton resonance. The dephasing time 200 fs, the time delay τ = 400 fs, and the pulse FWHM is 100 fs for both pulses. The peak value of the dipole coupling energy of the second pulse is $d_w E_1 = 0.1 E_R$, where the exciton binding energy E_R = 16 meV in CdSe. The corresponding peak amplitudes of the first pulse are shown with increasing dash length for $d_w E_1 = 0.01 E_R$, $0.03 E_R$, $0.05 E_R$, $0.07 E_R$, and for $0.1 E_R$ (solid line).

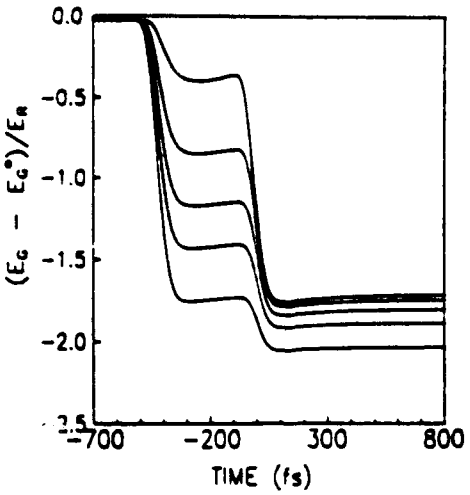

Figure 8. Renormalized band edge as a function time. E^0_G is the unrenormalized band edge. The different curves are $d_w E_1 = 0.01 E_R$, $0.03 E_R$, $0.05 E_R$, $0.07 E_R$, and $0.01 E_R$, from top to bottom, respectively. All parameters are the same as in Fig. 7.

CARRIER RELAXATION STUDIES IN SEMICONDUCTOR LASERS AND IN NOVEL GaAs QUANTUM-WELL STRUCTURES

N. Peyghambarian

PUBLICATIONS

N. Peyghambarian, S.W. Koch, A. Mysyrowicz, *Introduction to Semiconductor Optics* (Prentice Hall, Englewood Cliffs, New Jersey, 1993).

N. Peyghambarian, H.M. Gibbs, G. Khitrova, S.W. Koch and E.M. Wright, Optics and Photonics News **3**, 16 (1992).

P. Harten, A. Knorr, J.P. Sokoloff, F. Brown de Colstoun, S.G. Lee, R. Jin, E.M. Wright, G. Khitrova, S.W. Koch and N. Peyghambarian, "Propagation induced escape from adiabatic following in semiconductors," Phys. Rev. Lett. **69**, 852 (1992).

K. Meissner, B. Fluegel, H. Giessen, B.P. McGinnis, A. Paul, R. Binder, S.W. Koch, N. Peyghambarian, M. Grun and C. Klingshirn, "Spectral hole burning in the gain region of an inverted semiconductor," Phys. Rev. B Rapid Commun. **48**, 15472 (1993).

Y. Masumoto, B. Fluegel, K. Meissner, S.W. Koch, R. Binder, A. Paul and N. Peyghambarian, "Bandgap renormalization and optical gain formation in highly excited CdSe," J. Crystal Growth **117**, 732 (1992).

B.D. Fluegel, A. Paul, K. Meissner, R. Binder, S.W. Koch, N. Peyghambarian, F. Sasaki, T. Mishina and Y. Masumoto, "Experimental and theoretical investigation of femtosecond carrier relaxation in CdSe," Solid State Commun. **83**, 17 (1992).

T. Mishina, Y. Masumoto, B. Fluegel, K. Meissner and N. Peyghambarian, "Observation of coherent optical phonons in BiI_3," Phys. Rev. B **46**, 4229 (1992).

P.A. Harten, S.G. Lee, J.P. Sokoloff, J.R. Salcedo and N. Peyghambarian, "Noise in a dual dye jet hybridly mode-locked near infrared femtosecond laser," Opt. Commun. **91**, 465 (1992).

C.L. Chuang, R. Jin, J. Xu, P.A. Harten, G. Khitrova, H.M. Gibbs, S.G. Lee, J.P. Sokoloff, N. Peyghambarian, R. Fu and C.S. Hong, "GaAs/AlGaAs multiple quantum well nonlinear optical directional couplers," Int. J. Nonlinear Opt. Phys. **1**, 779 (1992).

M.F. Krol, T. Ohtsuki, G. Khitrova, R.K. Boncek, B.P. McGinnis, H.M. Gibbs and N. Peyghambarian, "All-optical high contrast GaAlInAs multiple quantum well asymmetric reflection modulator at 1.3 μm," Appl. Phys. Lett. **62**, 1550 (1993).

T. Ohtsuki, M.F. Krol, G. Khitrova, R. Jin, R.K. Boncek, B.P. McGinnis, H.M. Gibbs and N. Peyghambarian, "All-optical asymmetric Fabry-Perot reflection modulators," invited paper for Int. J. Nonlinear Opt. Phys. (Oct. 1993).

R. Jin, K. Okada, G. Khitrova, H.M. Gibbs, M. Pereira, S.W. Koch and N. Peyghambarian, "Optical nonlinearities in strained-layer InGaAs/GaAs multiple quantum wells," Appl. Phys. Lett. **61**, 1745 (1992).

R. Jin, M. Liang, G. Khitrova, H.M. Gibbs and N. Peyghambarian, Opt. Lett. **18**, 494 (1993).

R. Jin, D. Boggavarapu, G. Khitrova, H.M. Gibbs, Y.Z. Hu, S.W. Koch and N. Peyghambarian, Appl. Phys. Lett. 61, 1883 (1992).

F. Sasaki, T. Mishina, Y. Masumoto, B. Fluegel, K. Meissner and N. Peyghambarian, "Femtosecond optical nonlinearities under resonant excitation of excitons in CdSe," J. Crystal Growth 117, 768 (1992).

F. Sasaki, T. Mishina, Y. Masumoto, B. Fluegel, K. Meissner and N. Peyghambarian, "Nonequilibrium distribution of hot carriers in a CdSe thin film," Semicond. Sci. Technol. 7, B160 (1992).

N. Peyghambarian, "Femtosecond pulse propagation effects in semiconductors," QELS'93, May 2-7, 1993, Baltimore, Maryland (invited).

B. Fluegel, K. Meissner, A. Paul, S.W. Koch and N. Peyghambarian, "Femtosecond gain dynamics in a passive semiconductor," CLEO'93, May 2-7, 1993, Baltimore, Maryland.

B. Fluegel, K. Meissner, R. Binder, S.W. Koch and N. Peyghambarian, "Spectral hole burning in the gain region of an inverted semiconductor," ILS'93 Conference, October 3-8, 1993, Toronto, Canada (invited)

SCIENTIFIC PERSONNEL

R. Jin
P. Harten
B. Fluegel

DEGREES GRANTED

Brian Fluegel, PhD, 1992
Valorie Williams, PhD, 1991
Fred Jarka, MS, 1992
Paul Harten, PhD, 1992
Mark Krol, MS, 1992
C. C. Hsu, PhD, 1991

RESEARCH FINDINGS

The results we obtained during the course of this study are summarized below.

Adiabatic Following in Semiconductors

Adiabatic following is an off-resonant effect which occurs when the duration of a light pulse is less than the phase relaxation time T_2 and the magnitude of the pulse detuning is greater than its inhomogeneous linewidth. Under these conditions, the quantities in the optical Bloch equations which describe the system, namely the inversion and polarization, have a time dependence determined by the instantaneous amplitude of the light-pulse envelope, i.e., they follow the field.

The above conditions on the pulse duration and detuning can be satisfied in a semiconductor using femtosecond laser systems. This is most easily achieved for the exciton resonance in GaAs multiple-quantum-well structures (MQWs), which has a coherence time approaching one picosecond. The response of the exciton to a nonresonant light pulse can be described by the inversion and interband

polarization of the system using the semiconductor Bloch equations, which include the many-body Coulomb effects in time-dependent Hartree-Fock approximation. The numerical solution of these coupled equations not only explains the Stark shift, as shown previously, but also indicates that the system's inversion adiabatically follows the field. This aspect of the Stark effect is manifested experimentally in the time-resolved absorption measurements as a fast bleaching recovery of the exciton line.

Time-resolved pump-probe experiments were carried out using a synchronously pumped mode-locked dye laser with an average output power of 25 mW, 82 MHz repetition rate, and center wavelength tunable from 850 to 870 nm for room-temperature experiments. A colliding pulse mode-locked (CPM) dye laser amplified by copper vapor lasers (CVL) in cascade operating in 750 nm to 800 nm was employed for low-temperature ($\simeq$ 10 K) experiments. For this purpose, we first generated a continuum using CPM pulses amplified by CVL, and then the near-IR pulses were obtained by reamplifying the desired portion of the generated continuum using a second CVL. The autocorrelation of the pump pulse and the cross correlation of the pump and probe pulses in this case were 200 fs and 300 fs, respectively. The samples were molecular beam epitaxy (MBE) grown GaAs/$Al_xGa_{1-x}As$ multiple-quantum-well (MQW) and multiple-coupled-quantum-well (MCQW) structures with various well widths and barriers. In all room-temperature measurements the laser center wavelength was adjusted to allow detuning between four and five E_R below the heavy-hole exciton. Here E_R is the bulk GaAs Rydberg energy, i.e., 4.2 meV. The detunings for low-temperature measurements were smaller. The spectral transmission of the probe through the sample for different time delays between pump and probe was measured by an optical multichannel analyzer at the output of a spectrometer.

Figure 1(a) shows the low-temperature absorption spectrum of a GaAs MCQW sample for pumping below the exciton resonance and for different time delays, t_p, where t_p = t(probe) - t(pump). The solid curve represents the linear absorption, while the dotted spectrum corresponds to $t_p \neq 0$. It clearly shows that the heavy-hole exciton has been blue shifted and bleached. The dashed curve in Fig. 1(a), which corresponds to t_p = 500 fs, demonstrates that the blue shift and bleaching are mostly recovered. The complete recovery takes nanoseconds as a result of carrier generation caused mainly by the spectral overlap of the pump and the sample's absorption spectrum. The transient exciton blue shift is the manifestation of the optical Stark effect. This bleaching recovery is the signature of the transient adiabatic following.

For the analysis of our experiments, we used the semiconductor Bloch equations, i.e., the coupled equations of motion of the expectation value of the population of the state k and the interband polarization.

We solved the semiconductor Bloch equations numerically for different time delays, assuming constant dephasing and carrier-relaxation rates. The calculated spectrum for comparison with the room-temperature data of Fig. 1(a) is shown in Fig. 1(b). As in the experiment, the pump-pulse duration and detuning satisfied the adiabatic following conditions mentioned earlier. The temporal behavior of the exciton in Fig. 1(b) shows good qualitative agreement with the data. That is, the exciton both bleaches and shifts at negative time delays. The Stark shift, which reaches a maximum at a negative time, fully recovers after several hundred femtoseconds, while the bleaching, which is maximized at t_p = 0, does not quite completely recover.

Figure 2 shows the temporal behavior of the created carrier density along with the pump-pulse intensity. Note that similar to the experiments, there is a fast component of the density, which follows the pump, and a small long-lasting tail due to the incoherent component of the real carrier generation. The fast component is a result of the coherent response of the carrier density. It is the transient presence of this density which is responsible for the fast bleaching recovery. We assign this behavior to the ultrafast adiabatic following in semiconductors.

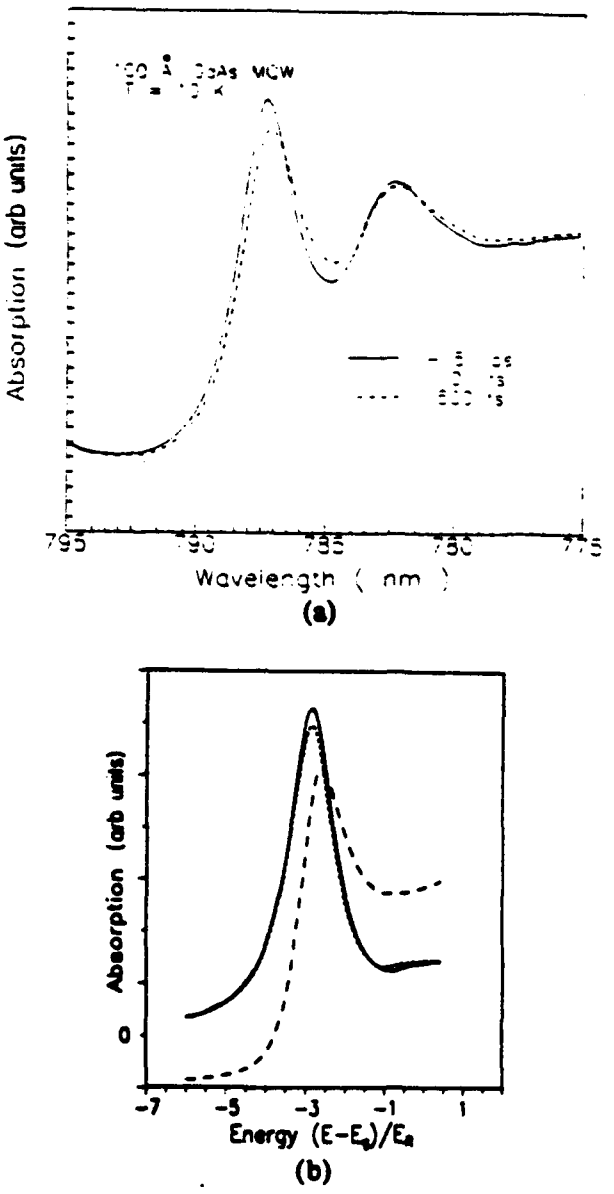

Figure 1. (a) Measured absorption spectra of a GaAs-AlGaAs MCQW at T = 10 K at different time delays. (b) Calculated absorption spectra for comparison with Fig. 1(a).

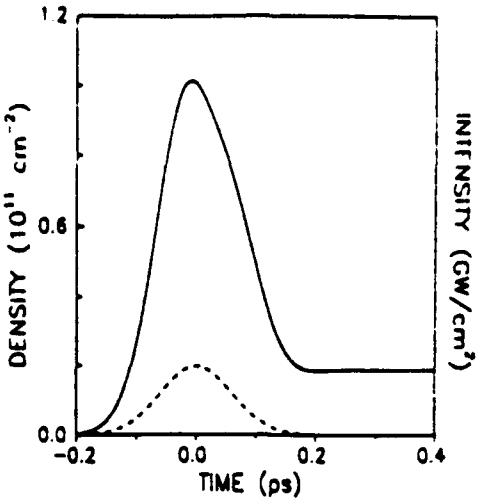

Figure 2. Calculated temporal behavior of the carrier density generated by pump pulse.

Femtosecond Nonequilibrium Carrier Relaxation in Bulk CdSe

A femtosecond spectral hole-burning technique was employed to study the relaxation of nonequilibrium carriers via carrier-carrier (CCS) and carrier-LO phonon (CPS) scattering. Excitation by 70-fs laser pulses several LO phonon energies above the exciton resonance at 10 K in CdSe results in a transient spectral hole that disappears in less than 100 fs. At the onset of the pump pulse we observed a nonthermal distribution that essentially extended from the pump energy of 1.99 eV to lower energies, indicating participation of both CCS and CPS as expected. The experiments were performed with 70-fs pulses generated at 1.99 eV from an amplified colliding pulse mode-locked dye laser. Figure 3(a) shows the linear absorption spectrum of the sample at 10 K. The two excitonic peaks labeled A and B originate from the heavy-hole and light-hole valence bands split by crystal field interaction. Absorption changes, $-\Delta\alpha$, following excitation by the pump pulse were measured as a function of time delay between the pump and probe pulses. Figure 4(a) shows $-\Delta\alpha$ spectra in 50-fs intervals. The 0-fs and 50-fs spectra show the presence of a hot nonthermal spectral hole, as indicated by the hatched area, on the high-energy side of A and B exciton bleaching. As the nonthermal distribution thermalizes, the spectral hole washes out and only the bleached excitons remain.

Our theoretical analysis was based on the semiconductor Bloch equations. CCS and CPS were included in the carrier collision rates, and screening was treated quasi-statically. Results of our theory are presented in Figs. 3(b) and 4(b). Figure 3(b) shows the calculated linear absorption spectrum, consisting of the A and B excitons. The 0-fs spectrum in Fig. 4(b) clearly displays the spectral hole peaked at the pump position 12 E_R, where E_R = 15.75 meV, the A-exciton Rydberg energy. The two excitons are completely bleached. The hole has a tail extending to low energies with respect to pump energy, as was observed in Fig. 4(a), in good agreement with the experiment. The theory also shows that the spectral hole washes out by 100 fs, and the excitons stay bleached for later times, indicating very large carrier-carrier scattering rates. Our analysis shows how the very short scattering times (both the CCS and the CPS) yield an almost instantaneous bleaching of both the exciton resonance and the Coulomb enhancement of the lower continuum states. Since the LO-phonon emission processes are essentially as fast as the CCS, the Pauli blocking (spectral hole) primarily affects the low-energy side of the pump frequency. After approximately a hundred femtoseconds, the phase-space blocking is similar

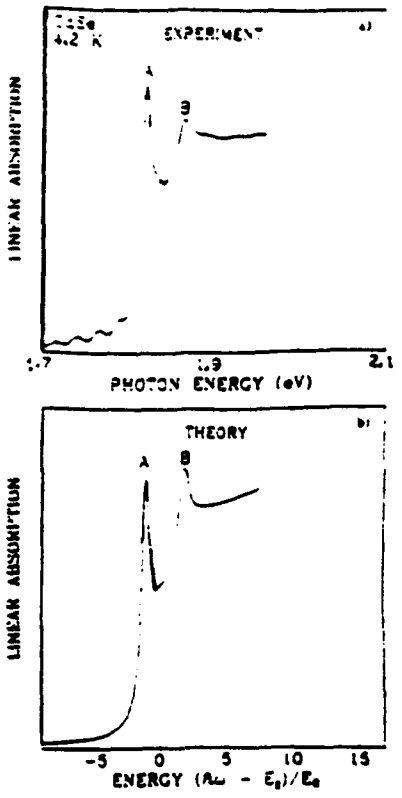

Figure 3. (a) The measured linear absorption of our CdSe platelet at 10 K. (b) The calculated linear absorption.

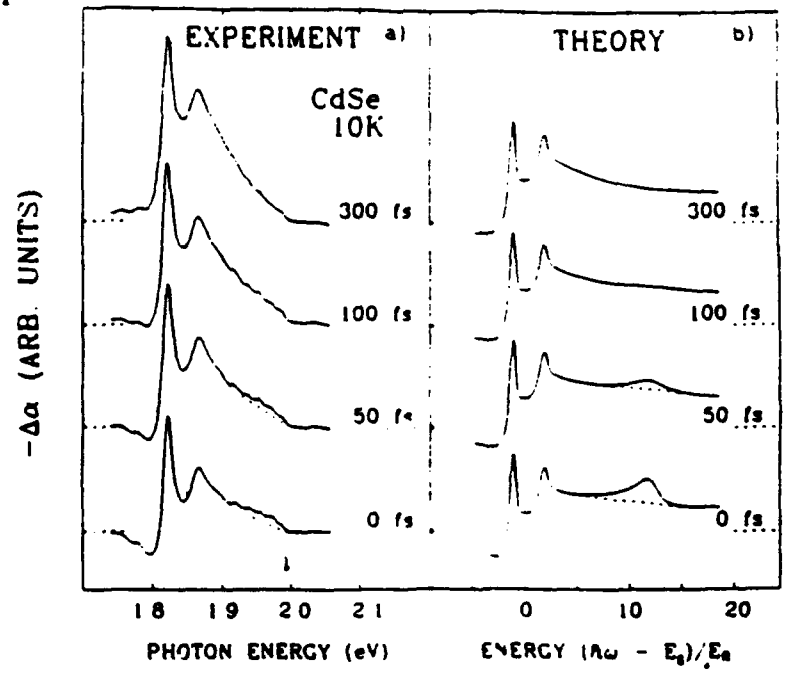

Figure 4. (a) The measured change in the absorption coefficient observed under the 1.99 eV excitation at 10 K. The time delay of each spectrum is shown in the figure. The hatched area shows the nonthermalized distribution of hot carriers. (b) Calculated pump-induced absorption for various time delays bewteen the pump and probe pulses.

to that of a high-temperature thermal plasma where, in this case, the temperature range is essentially given by the LO-phonon energy. This is a result of both CPS and CCS, where the CPS reduces the mean kinetic energy of the plasma, and the CCS yields a quasi-thermal distribution where even the states below $\hbar\omega_{LO}$ are filled. The most prominent effect of the phase-space blocking of the low k-states is the reduction of the absorption increase below the A-exciton, which in the experimental data sets in after 100 fs. In this investigation, the experimental results seem to be well-explained within the simple model of equilibrium phonon distributions. An enhanced temporal resolution, however, might prove the significance of nonequilibrium and/or coherent phonon effects.

Coherent Phonon Excitation in Semiconductors

BiI_3 is a layered semiconductor with two-dimensional excitons trapped by stacking faults. These excitons, labeled as R, S, and T, are extremely sharp, with long T_2 times, as shown in Fig. 5. Monitoring the absorption change at the peaks of R, S, and T excitons resulted in an interesting observation shown in Fig. 6. An oscillatory signal is detected at the R, S, and T peaks and at a wavelength of 630 nm, which is in the transparency region of the semiconductor. We verified that these oscillations are *not* the result of Rabi flopping because of the presence of the signal at 630 nm, and also because the signal lasts for $\simeq$30 ps. They cannot be the result of quantum beats between the excitons either because the frequency of oscillations does not correspond to the energy separation of any of the excitons. The energy separation of $\simeq$14.3 meV observed in these oscillations precisely matches the TO phonon frequency in BiI_3. Thus, we concluded that our data arise from a coherent excitation of TO phonons in the medium, presumably by *impulse stimulated* Raman scattering process. The $\simeq$30-ps decay time for the oscillations then is due to the vibrational dephasing as a result of coupling with incoherent phonons in this two-dimensional system.

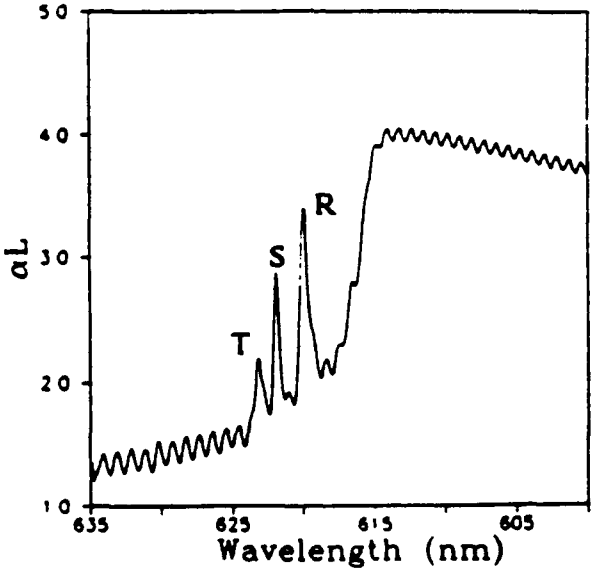

Figure 5. Linear absorption spectrum of BiI_3 at T = 10 K. R, S, and T correspond to the three-stacking-fault excitons in this layered semiconductor.

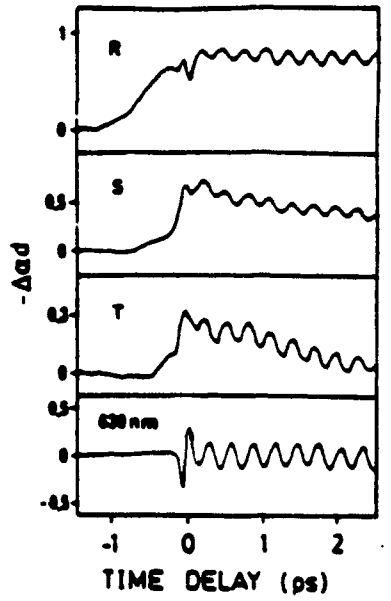

Figure 6. The measured change in absorption for the R, S, and T excitons and the transparency region at 630 nm of the BiI_3 sample of Fig. 5.

Femtosecond Pulse Propagation in Semiconductor Waveguides

We observed a new, interesting effect that we called "propagation-induced escape from adiabatic following" in a GaAs-AlGaAs waveguide. This observation, which agreed well with our theory, indicates that high-intensity femtosecond pulses break up as they propagate through a semiconductor when they are tuned below the exciton resonance. This pulse breakup results from the escape of the system from adiabatic following regime as the pulse propagates through the material. The summary of results of this work may be found in P. Harten et al., Phys. Rev. Lett. **69**, 852 (1992).

Spectral Hole Burning in the Gain of an Inverted Semiconductor

We have obtained unambiguous experimental evidence for the presence of a spectral hole in the gain region of an inverted semiconductor. A three-beam femtosecond experiment was performed for this study. The first femtosecond laser beam was used as the "gain" beam, whose function was to generate high-density electron-hole pairs to invert the semiconductor and produce the gain region. Thus, the material was pumped optically, not electrically. The two other femtosecond laser beams were the pump pulse to pump inside the gain region and a broadband probe pulse to detect the changes made by the pump. The broad probe allowed monitoring of the entire gain region of the semiconductor simultaneously. We observed spectral holes that persisted for the duration of the pump. These holes moved with the pump frequency as the pump tuned across the gain region, as expected. Figure 7 shows a typical example of the hole-burning results where the presence of the burned hole is clearly seen, and its disappearance in less than 200 fs is demonstrated. The incident pulse duration was $\simeq$ 100 fs.

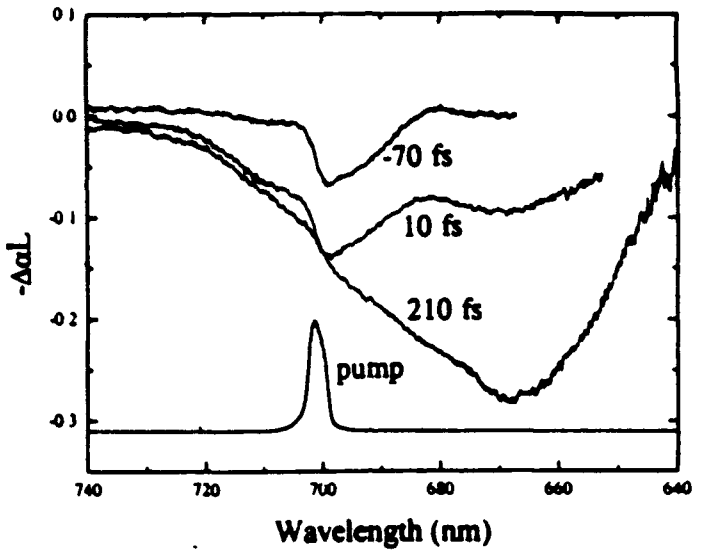

Figure 7. The observed change in the gain of an inverted semiconductor as a result of pumping inside the gain region. The hole is generated after pumping and disappears in less than 200 fs.

SPECTRAL HOLE BURNING AND INSTABILITIES IN SEMICONDUCTOR LASERS

M. Sargent III and S.W. Koch

PUBLICATIONS AND PRESENTATIONS

W.W. Chow, M.F. Pereira and S.W. Koch, "A many-body treatment of the modulation response in a strained quantum well semiconductor laser medium," Appl. Phys. Lett. **61**, 758 (1992).

R. Jin, D. Boggavarapu, G. Khitrova, H.M. Gibbs, Y.Z. Hu, S.W. Koch and N. Peyghambarian, "The linewidth broadening factor of a microcavity semiconductor laser," Appl. Phys. Lett. **61**, 1883 (1992).

M. Sargent III, S.W. Koch and W.W. Chow, "Sidemode gain in semiconductor lasers," J. Opt. Soc. Am. B **9**, 1288 (1992).

M. Rose, M. Lindberg, W.W. Chow, S.W. Koch and M. Sargent III, "Composite-cavity-mode approach to single-mode semiconductor laser feedback instabilities," Phys. Rev. A **46**, 603 (1992).

S.W. Koch and W.W. Chow, "Microscopic theory and modelling of semiconductors and semiconductor lasers," invited article for *Trends in Optical Engineering*, publ. by Research Trends, Council of Scientific Research Integration, India (1993).

F. Jahnke, S.W. Koch and K. Henneberger, "Dynamic response of short-cavity semiconductor lasers," Appl. Phys. Lett. **62**, 2313 (1993).

F. Jahnke, K. Henneberger, W. Schäfer and S.W. Koch, "Transient nonequilibrium and many-body effects in semiconductor microcavity lasers," J. Opt. Soc. Am. B **10**, 2394 (1993).

P. Ru, J.V. Moloney, R. Indik, S.W. Koch and W. Chow, "Microscopic modelling of bulk and quantum well GaAs-based semiconductor lasers," Optics and Quantum Electronics (submitted).

SCIENTIFIC PERSONNEL

M. Sargent III
F. Jahnke

RESEARCH FINDINGS

In this project we concentrated on a microscopic analysis of semiconductor gain media, semiconductor lasers, and laser instabilities such as spectral and kinetic hole burning. Given the relatively small amount of research funding through JSOP, it is probably fair to say that this project led to a very substantial number of results in the semiconductor laser arena.

In addition to the results that were highlighted in our earlier research and progress reports, during the last part of this project we concentrated on the development and extension of a truly quantum mechanical nonequilibrium theory of semiconductor lasers with a special emphasis on the novel microcavity laser structures, such as vertical cavity surface emitting lasers (VCSELs) or the microdisk whispering gallery mode lasers.

For these microcavity lasers, we investigated the influence of many-body, nonequilibrium, and cavity effects, and the emission characteristics and laser lineshape. For many operating conditions we find that the electron-hole plasma in these devices is in a genuine nonequilibrium state. The blocking of

the carrier states in the gain region leads to a pumping that has maximum efficiency in energetically high lying states. Hence, the pumping produces carriers with a higher than average kinetic energy.

At the same time, the lasing, which takes place close to the center of the gain region, removes carriers with less than average kinetic energy. The competition between the different timescales, i.e., the carrier cooling time on the one hand and the stimulated carrier lifetime on the other, determines the resulting nonequilibrium carrier distribution. If the stimulated recombination time is shorter than the cooling time, we encounter kinetic hole burning and substantial carrier heating, which can cause electron-hole-plasma temperatures that exceed the lattice temperature by as much as 300 K.

In our investigations of the linewidth of the laser emission, we used our self-consistent, fully quantum mechanical nonequilibrium laser theory to compute the spectral emission characteristics of semiconductor microcavity lasers as a function of the pump intensity. Our approach is allows us to predict the laser emission spectrum starting from the spontaneous emission, well below threshold, all the way to the stimulation dominated emission, well above threshold. These calculations have been done for a number of different pumping conditions (i.e., injection pumping or optical pumping with various excess energies) and different resonator conditions. These resonator conditions influence the amount of spontaneous emission that is coupled into the laser mode.

As one of the most striking results, we find (in agreement with experimental observations by R. Slusher et al. at AT&T Bell Labs) that the usual Shawlow-Townes line narrowing for increasing laser intensity does not occur in microcavity lasers with high spontaneous emission coupling efficiency. Due to the substantial contribution of the spectrally broad spontaneous emission, for the high coupling case we find that the laser linewidth rapidly saturates with increasing intensity and stays more or less constant, the spectral width being determined primarily by the width of the cavity resonance under the realized inversion conditions.

In summary, our theoretical analysis clearly demonstrates the necessity to include the quantum mechanical many-body and Coulomb effects into a consistent analysis of microcavity lasers. Based on this approach, a number of experimentally relevant modifications of the laser characteristics have been predicted, and (partially) experimentally verified. Even though this project will no longer be funded under JSOP, we will continue our investigations to obtain a coherent understanding of the light-matter interactions taking place in semiconductor lasers.

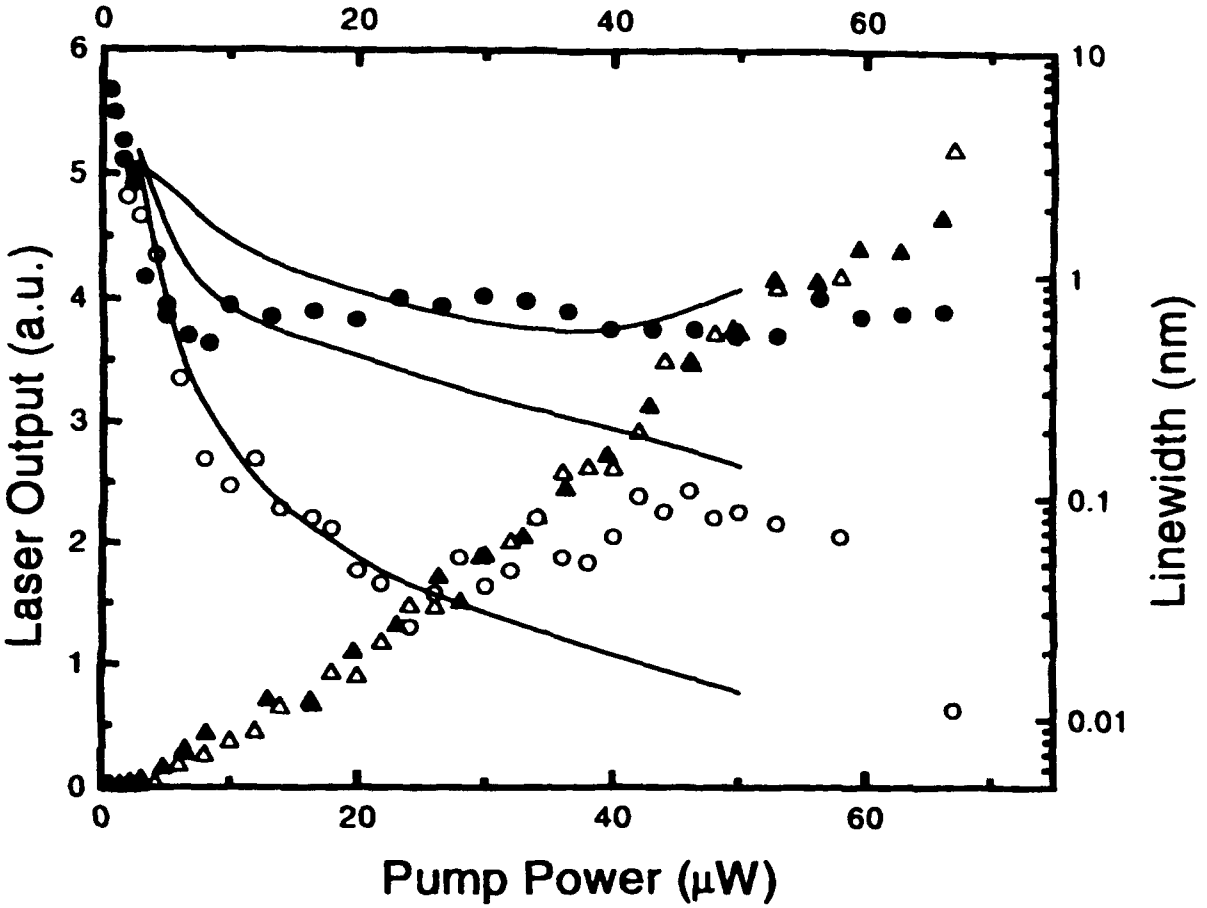

Figure 1. Comparison of the experimental (open and solid symbols) and theoretical (lines) results for the linewidth and output intensity of microdisk lasers. The solid data points are for a 2.2-μm diameter microdisk (spontaneous emission coupling measured to be 0.1-0.3), and the open points are for a 5-μm diameter microdisk (spontaneous emission coupling measured to be 0.02-0.05). The theoretical results are for spontaneous emission couplings of 0.4, 0.1, and 0.01 (from top to bottom).

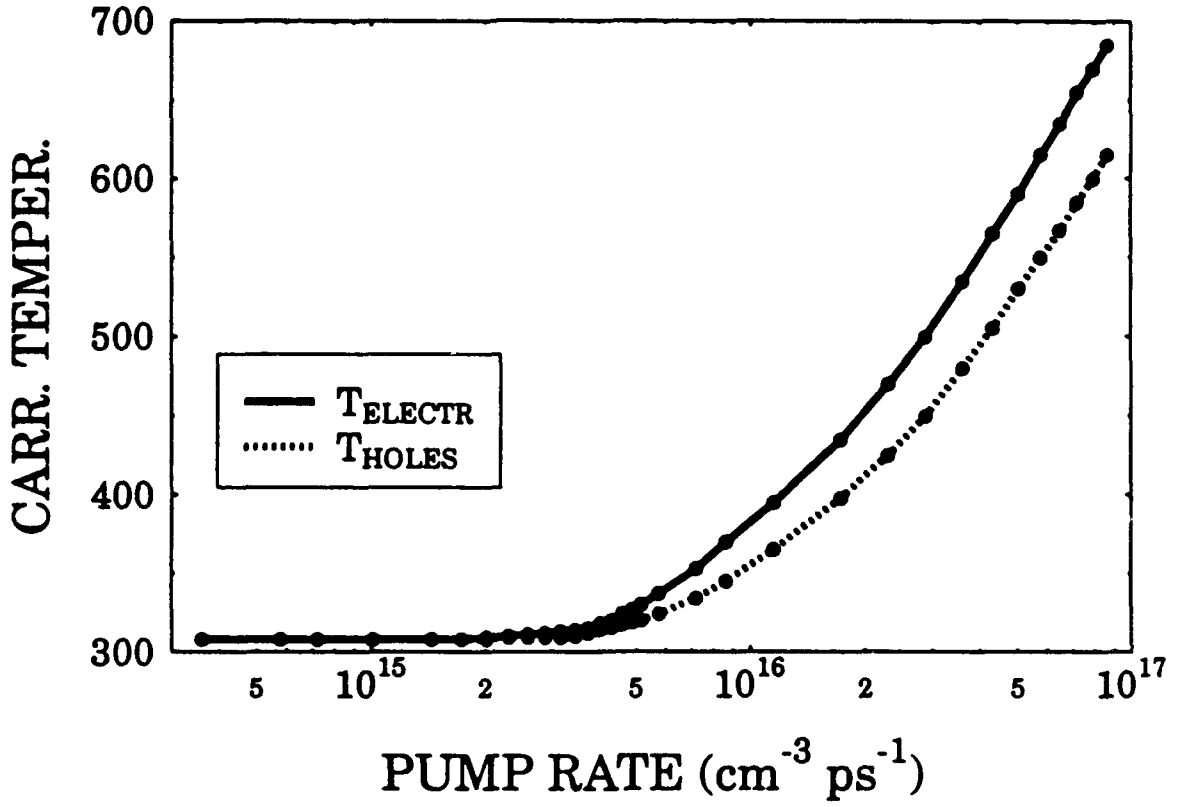

Figure 2. Effective carrier temperature versus pump rate for carrier injection pumping of a microcavity laser with a cavity length of 1 μm and effective mirror reflectivity of 99%.

SURFACE PHOTOVOLTAGE OF SEMICONDUCTOR STRUCTURES

D. Sarid, M. Gallagher and T. Ruskell

PUBLICATIONS

M.J. Gallagher, T.G. Ruskell, D. Chen, D. Sarid and H. Jenkinson, "Nanosecond time-scale semiconductor photoexcitations probed by a scanning tunneling microscope," Appl. Phys. Lett. **64**, 256 (1994).

D. Sarid, *Scanning Force Microscopy*, New York: Oxford University Press, Revised Edition, in press.

DEGREES AWARDED

Mark J. Gallagher, Ph.D, November 12, 1993

RESEARCH FINDINGS

This research was aimed at characterizing semiconductor nanostructures with an STM using intense optical fields. We have developed a novel approach of probing fast optical interactions using the scanning tunneling microscope (STM). We have demonstrated the feasibility of this technique by using beat frequencies of longitudinal modes of a HeNe laser at the tunneling junction[1] by presenting the fast optical response of photoexcited charge carriers in the layered structure semiconductors *n*-type MoS_2 and *p*-type WSe_2. These experiments open the door to a new and exciting field of optics that takes advantage of the short time response of the STM junction, which is several *femtoseconds*.

The termination of our JSOP funding has put this project in jeopardy; however, we are continuing to develop the technology of locally probing the optical response of carriers in quantum well structures, quantum dots and other nanostructures.[2-8] Our laboratory has achieved the shortest time response of an STM using optical excitations (2.3 nsec) of semiconductors, and is one of only a few laboratories in the United States to perform such experiments. The experiments so far have been conducted in ambient, using layered semiconductors. However, we have just finished constructing a special UHV-STM facility that is now fully operational. We are currently moving this experiment into the UHV-STM facility. Our specific plans call for intensifying the research using the following methods: (1) incorporating the experiment into our new optically integrated UHV-STM facility; (2) using an Ar-pumped dye laser for wavelength scans; and (3) using the different modes of the laser to probe the temporal response of the carriers. The samples to be used will be nanolithographically machined semiconductor and metal-semiconductor structures and cleaved multiple quantum well structures.

A revised edition of my book[9] *Scanning Force Microscopy* has been written in the course of this project, and will be published by Oxford University Press in May 1994.

REFERENCES

1. M.J. Gallagher, T.G. Ruskell, D. Chen, D. Sarid and H. Jenkinson, "Nanosecond time-scale semiconductor photoexcitations probed by a scanning tunneling microscope," Appl. Phys. Lett. **64**, 256 (1994).

2. D. Sarid, B.P. McGinnis and T.D. Henson, "Four-wave mixing and scanning tunneling microscopy of semiconductor clusters," SPIE **881**, 114 (1988).

3. D. Sarid, T.D. Henson, L.S. Bell and C.J. Sandroff, "Scanning tunneling microscopy of semiconductor clusters," J. Vac. Sci. Technol. A **6**, 424 (1988).

4. D. Sarid, T.D. Henson, N. Armstrong and L.S. Bell, "Probing of basal planes of MoS_2 by scanning tunneling microscopy," Appl. Phys. Lett. **52**, 2252 (1988).

5. T.D. Henson, D. Sarid and L.S. Bell, "Scanning tunneling microscopy of layered-structure semiconductors," J. Microscopy **152**, 467 (1988).

6. T. Iwabuchi, C. Chuang, G. Khitrova, M.E. Warren, A. Chavez-Pirson, H.M. Gibbs, D. Sarid and M. Gallagher, "Fabrication of GaAs nanometer structures by dry etching," SPIE **1284**, 142 (1990).

7. S. Howells, M. Gallagher, T. Chen and D. Sarid, "Oxidation effects on cleaved multiple quantum well surfaces in air observed by scanning probe microscopy," Appl. Phys. Lett. **61**, 801 (1992).

8. M.J. Gallagher, S. Howells, L. Yi, T. Chen and D. Sarid, "Photon emission from gold surfaces in air using scanning tunneling microscopy," Surf. Sci. **278**, 270 (1992).

9. D. Sarid, *Scanning Force Microscopy*, New York: Oxford University Press, Revised Edition, May 1994.

PROPAGATION OF SHORT OPTICAL PULSES IN PASSIVE AND ACTIVE NONLINEAR ALL-OPTICAL SWITCHES

E.M. Wright

PUBLICATIONS

A. Knorr, R. Binder, E.M. Wright and S.W. Koch, "Amplification, absorption, and lossless propagation of femtosecond pulses in semiconductor amplifiers," Opt. Lett. **18**, 1538 (1993).

A. Knorr, R. Binder, E.M. Wright and S.W. Koch, "Absorption of high intensity pulses in semiconductor amplifiers," Optics & Photonics News, OPTICS '93, 44 (December 1993).

N. Peyghambarian, E. Hanamura, S.W. Koch, Y. Masumoto and E.M. Wright, "Optical characterization and applications of semiconductor quantum dots," in A.S. Edelstein and H. Hahn, eds., *Nanostructured Materials: Synthesis, Characterization, and Uses*, (Adam Hilger, 1993).

P. Varatharajah, J.V. Moloney, A.C. Newell and E.M. Wright, "Stationary nonlinear waves guided by thin films bounded by nonlinear diffusive Kerr media," J. Opt. Soc. Am. B **10**, 46 (1993).

E.M. Wright, R.J. Hawkins and R.J. Deri, "Coupled-mode theory of vertically integrated impedance-matched waveguide/photodetectors," submitted to IEEE J. Quant. Electron., 1993.

J. Powell, E.M. Wright and J.V. Moloney, "Reflection of localized beams from a nonlinear absorbing interface," to be published in SIAM J. Appl. Math., 1993.

E.M. Wright, "Coupled-mode theory of vertically integrated impedance-matched waveguide/photodetectors," Topical Meeting on *Integrated Photonics Research*, Palm Springs, 1993, contributed paper.

N.P. Peyghambarian, B.P. McGinnis, P.A. Harten, A. Knorr, S.G. Lee, R. Jin, F. de Colstoun, E.M. Wright, G. Khitrova, H.M. Gibbs and S.W. Koch, "Femtosecond pulse propagation effects in semiconductors," QELS, Baltimore (1993), invited paper.

R. Binder, A. Knorr, E.M. Wright and S.W. Koch, "Amplification, absorption, and soliton-like propagation of femtosecond pulses in semiconductor gain media," CLEO, Baltimore, 1993, contributed paper.

E.M. Wright, "Ultrashort pulse propagation in ocular and related media," *Nonlinear Optics Workshop*, Tucson, September 1993, invited paper.

E.M. Wright, invited paper, "Quantum dot figure of merit for all-optical switching applications," 184th Meeting of the Electrochemical Society, New Orleans (October, 1993).

R. Binder, A. Knorr, E.M. Wright and S.W. Koch, invited paper, "Gain and absorption in semiconductor amplifiers," 184th Meeting of the Electrochemical Society, New Orleans (October, 1993).

SCIENTIFIC PERSONNEL

Ewan M. Wright

RESEARCH FINDINGS

Our recent research has been in the areas of femtosecond pulse propagation in semiconductor amplifiers and all-optical switching using quantum dots semiconductor materials. This work has been published in several journal articles, a book chapter, and has been presented at several scientific meetings.

Investigations of femtosecond pulse propagation in semiconductor amplifiers has continued due to potential applications to all-optical switching. In particular, the propagation of fs pulses is radically different from ps pulses. For ps or longer pulses, gain saturation provides an adequate physical basis for understanding pulse propagation: here only amplification of the output energy with respect to the input can occur. At high input intensities, the gain is saturated as the carrier density approaches the transparency value where gain equals loss. In the gain saturation model it is assumed that the electron and hole distribution functions remain Fermi-Dirac distributions with fixed temperature but variable density. This model is therefore only valid if the pulse duration greatly exceeds the carrier redistribution time. We have observed extreme departures from this behavior in numerical simulations in which high intensity 100 fs pulses are absorbed in semiconductor amplifiers. This can occur since the carrier distribution functions are driven far from equilibrium with a large concomitant increase in the carrier temperature (from 300 K to 600 K in the simulations). This increase in the carrier temperature leads to a reduction in the gain and to absorption at high input intensity. At a certain critical input intensity the gain and loss are balanced and the pulse propagates in a loss-less manner, reminiscent of the solitons of self-induced transparency.

For all-optical switching applications a medium with a large nonlinear refractive-index is sought while at the same time minimizing the detrimental effects of absorption. In material terms this calls for a system whose resonance conditions can be varied so that the tradeoff between refractive-index and absorption can be adjusted for a given laser frequency. Our recent work shows that this degree of flexibility is realized in quantum dots since the quantum confinement leads to a tunable blue-shift in the lowest exciton resonance which increases with decreasing dot radius. In particular, in collaboration with Prof. S.W. Koch we have calculated the all-optical switching figure of merit for a variety of quantum dots materials using a microscopic semiconductor model. These results show explicitly that quantum dots are good candidates for all-optical switching applications.

ATOM OPTICS

P. Meystre

PUBLICATIONS AND PRESENTATIONS

T. Zaugg, M. Wilkens, P. Meystre and G. Lenz, "Adiabatic atomic cooling in microwave cavities," Opt. Commun. **97**, 189 (1993).

M. Wilkens, E. Goldstein, B. Taylor and P. Meystre, "A Fabry-Pérot for atoms," Phys. Rev. A **47**, 2366 (1993).

G. Lenz, P. Pax and P. Meystre, "Exchange force in the near-resonant Kapitza-Dirac effect," Phys. Rev. A **48**, 1707 (1993).

G. Lenz and P. Meystre, "Resonance fluorescence from two identical atoms in a standing-wave field," Phys. Rev. A **48**, 3365 (1993).

G. Lenz, P. Meystre and E. M. Wright, "Nonlinear atom optics," Phys. Rev. Lett. **71**, 3271 (1993).

T. Zaugg, M. Wilkens and P. Meystre, "Back-action in the measurement of macroscopic superpositions in microwave cavities," Found. Phys. **23**, 857 (1993).

T. Zaugg, P. Meystre, G. Lenz and M. Wilkens, "Theory of adiabatic cooling in cavities," Phys. Rev. A, in press.

P. Meystre, "The Jaynes-Cummings model is alive and well," in W.T. Grandy and P.W. Milonni, eds., *Physics and Probability*, (Cambridge University Press, 1993), p. 49.

P. Meystre and M. Wilkens, "Spontaneous emission by moving atoms," in P. Berman, ed., *Cav*)*ED*, (Academic Press, 1994).

T. Zaugg, G. Lenz and P. Meystre, "Adiabatic atomic cooling in cavity QED," in F. Ehlotzky, ed., *Fundamentals of Quantum Optics III*, (Springer Verlag, Heidelberg, 1993), p. 185.

P. Meystre, "A diabatic cooling in microwave cavities," Third International Seminar on Fundamentals of Quantum Optics, Kühtai, Austria, 1993.

P. Meystre, "Nonlinear atom optics," Workshop on New Theoretical Methods in Quantum Optics, Boulder, Colorado, 1993.

P. Meystre, "Atom optics," Sixteenth Congress of the International Commission for Optics, Budapest, Hungary, 1993.

P. Meystre, "Toward nonlinear atom optics," Annual Meeting, Optical Society of America, Toronto, Canada, 1993.

T. Zaugg, G. Lenz and P. Meystre, "Adiabatic atomic cooling in cavities," Annual Meeting, Optical Society of America, Toronto, Canada, 1993.

G. Lenz and P. Meystre, "Resonance fluorescence from two identical atoms in a standing wave," Annual Meeting, Optical Society of America, Toronto, Canada, 1993.

RESEARCH FINDINGS

Considerable progress has been made towards understanding the physics of laser cooled and trapped atoms. One example is the recent observation of quantized atomic motion in one-, two-, and three-dimensional optical lattices.[1,2,3,4] The new and detailed understanding of the mechanical aspects of light/matter interactions has already lead to the suggestion of mechanisms by which atomic samples with temperatures in the nanoKelvin, and possibly picoKelvin, regime may be prepared.

The study of the physics of ultracold atoms opens up a broad new field of fundamental and applied research. It plays an essential role in understanding the fundamental limitations of atomic cooling, and hence of devices such as atomic clocks: the many-body effects that are predicted to occur when the atomic temperature is near the recoil limit are bound to lead to shift and broadening mechanisms, and possibly nonlinear heating, thereby influencing the achievable performance of these devices. Many-body effects are expected to be important in lithographic applications as well, whose basic principles are closely related to those of optical lattices: to achieve reasonable writing speeds, high atomic densities will clearly be required.

In addition to these immediate practical concerns, the availability of ultracold atoms is of considerable interest in atom interferometry, since it naturally leads to the possibility of coherently splitting atomic wave functions with a large separation between the arms of the interferometer. Such macroscopic separations are highly desirable since most applications of atom interferometry require that the arms of the interferometer be placed in different environments and/or that large areas be covered by the interferometers, as e.g. in gyroscopic applications. Cold atoms also have profound implications in the physics of collisions, since they lead us to a regime where standard approximations cease to be valid.[5]

The net effect of any two-body interaction $V_{12}(R)$ is given by its overlap with the atomic wave functions, properly symmetrized in the case of indistinguishable particles. For short-range interactions, a sizeable overlap between the atomic wave functions, and hence a high atomic density, is necessary to achieve noticeable effects, but in the case of the long-range dipole-dipole interaction between coherently driven atoms, many-body effects can be expected already at relatively modest densities. In this situation, it becomes incorrect to treat the atoms in the sample as independent. Rather, many-body effects lead to an effective nonlinear behavior of the single atoms. This regime, which we call "nonlinear atom optics," is to de Broglie optics what nonlinear optics is to conventional optics. It suggests that novel effects such as the generation of atomic solitons and solitary waves, atomic wave mixing, and atomic phase conjugation could be possible. In addition, sufficiently high atomic densities in optical lattices could lead to spontaneous pattern formation and the creation of other stable long-range structures, such as possibly superlattices. Even more intriguing, perhaps, is that the combination of nonlinearities with dissipation, in the form of spontaneous emission, and of a "pump" mechanism, might suggest the possibility of a "coherent atomic beam generator," which could loosely be considered as the atom optics equivalent of a laser.

During this year, we have initiated a theoretical program to study these effects. This is a high-risk, high-pay-off task in nearly virgin territory, where two major avenues of investigation are possible. The first one consists of concentrating one's efforts on the understanding of the dynamics of the system at the microscopic level. In practice, two atoms are about as much as can be handled in this approach, which reduces then to the theory of diatomic collisions between ultracold atoms. This challenge is presently being tackled in particular at NIST, in the group of Dr. Julienne.

We have chosen, instead, a more "phenomenological" approach, paying relatively little attention to the detailed way the atoms interact at the microscopic level, and concentrating on more "global" effects

such as the generation of solitons and spatial patterns, phase transitions, etc. In the absence of a detailed understanding of cold atom collisions, such an approach has considerable merit in permitting one to investigate the possible effects of these two-body interactions in a *sample* of ultracold atoms. In this case, the specific form of the two-body interaction is considered, in a sense, as a "free parameter," and predictions about the behavior of the system can be made for various forms of the potential.

The general many-body Hamiltonian including a two-body interaction can be expressed in a standard way as

$$\begin{aligned}\hat{\mathcal{H}} &= \int d1d2\,\langle 1|H_0|2\rangle\hat{\psi}^\dagger(1)\hat{\psi}(2) \\ &+ \frac{1}{2}\int d1d2d3d4\langle 1,2|V|3,4\rangle\hat{\psi}^\dagger(1)\hat{\psi}^\dagger(2)\hat{\psi}(4)\hat{\psi}(3) \\ &= \hat{\mathcal{H}}_0 + \hat{V}\,.\end{aligned} \tag{1}$$

Here, H_0 is the single-particle Schrödinger Hamiltonian, and includes the atom-field dipole interaction, the electromagnetic field being either classical or quantized, and V is the two-body dipole-dipole potential. All kets $|\ell\rangle$ give a complete description of the single atom states, i.e. they include both the center-of-mass and the internal quantum numbers. We use numbers to indicate dummy variables and letters to label a specific state. The state $|\ell\rangle$ is obtained by application of the creation operator $\hat{\psi}^\dagger(\ell)$ to the atomic vacuum $|0\rangle$, $\hat{\psi}^\dagger(\ell)|0\rangle = |\ell\rangle$, where $[\hat{\psi}(\ell),\hat{\psi}^\dagger(\ell')] = \delta(\ell-\ell')$ for bosons, and the δ-function should be interpreted as a product of δ-functions for continuous quantum numbers and Kronecker deltas for discrete ones. A normalized N-particle state $|\psi\rangle_N$ is obtained as

$$|\psi\rangle_N = \frac{1}{\sqrt{N!}}\int d1...dN f_N(1,2,...,N)\hat{\psi}^\dagger(N)...\hat{\psi}^\dagger(1)|0\rangle\,, \tag{2}$$

where the N-body wave function $f_N(1,2,...,N)$ is totally symmetric in its arguments.

In general, the many-body problem described by the Hamiltonian (1) cannot be solved exactly. There are, however, a number of approximate techniques that have been developed. For the bosonic problem at hand, time-dependent Hartree techniques originally utilized in nuclear physics seem particularly attractive. The central tenet of the Hartree approximation consists in factorizing the N-body wave function $f_N(1,...,N)$ as a product of effective single-particle wave functions. In the time-dependent Hartree approximation, the equations of motion for the effective single-particle states are determined from the Hartree variational principle.[6] This yields the system of effective single-particle nonlinear Schrödinger equations

$$\begin{aligned}i\hbar\frac{\partial\phi_N(\ell)}{\partial t} &= \int d2\,\langle\ell|H_0|2\rangle\,\phi_N(2) \\ &+ (N-1)\int d1d2d3\,\langle\ell,1|V|2,3\rangle\,\phi_N^*(1)\phi_N(2)\phi_N(3).\end{aligned} \tag{3}$$

Equations (3) form the basis of nonlinear atom optics. They show that, *from the perspective of a single atom, the N - 1 other bosonic atom effectively act as a nonlinear medium.* This is analogous to the situation in conventional nonlinear optics, where the presence of a medium can lead to an effective nonlinear behavior of the light field when the medium dynamics is traced over.

Equations (3) are quite general, as the single-particle Hamiltonian H_0 could describe the interaction between atoms and a standing-wave field, their interaction with a magneto-optical trap, the potential of an optical lattice, or any situation that does not involve many-body effects. Also, the atoms could be simple two-level or multi-level systems as are required in most standard laser cooling schemes.

We have already analyzed[7] a number of consequences of Eqs. (3). In particular, for the case of two-level atoms interacting with a near-resonant light field, the so-called near-resonant Kapitza-Dirac

effect, we predict modifications of the conventional Pendellösung of Bragg scattering. In another regime, the problem is reduced to a classical massive Thirring model, with the possibility of generating atomic Thirring solitons. In one dimension, gap solitons as well as nonlinear focusing effects are expected to occur. Furthermore, if the equations of nonlinear atom optics are transformed to momentum space they reveal a variety of four-wave-mixing terms including those responsible for phase conjugation. This suggests the possibility of an atomic phase conjugator capable of reconstructing, or time-reversing, atomic wave functions.

Turning now to the question of numbers, we note that nonlinear effects are expected to become noticeable as soon as the effective nonlinearity $(N-1)V_0|\phi|^2/q$ becomes comparable to the effects of linear diffraction, whose strength is of the order $\hbar^2q^2/2M$. Stated differently, this indicates that nonlinear effects should arise as soon as the two-body interaction energy becomes comparable to the photon recoil energy. For the long-range dipole-dipole interaction and at resonance, this yields the critical linear density $\rho_L \simeq N/L \simeq w_0 q/\beta\gamma$. Here β is a geometrical factor that reflects the fact that the effective strength of the dipole-dipole interaction is given by the fraction of spontaneously emitted photons that can be reabsorbed by atoms inside the laser beam. For the Cesium D_2-line, we have $\rho_L \simeq 30/\beta$ cm^{-1}, which corresponds to relatively modest densities of $\rho \simeq 3 \cdot 10^{10}$ cm^{-3} for $\beta = 10^{-2}$. Clearly, these numbers are consistent with the experimental observation that cooling ceases to follow single atom scaling laws for the densities that can now be achieved in the lab.[8,9,10] A very important point here is that nonlinear effects are expected to occur much before the occurrence of Bose condensation, and hence experiments are possible without major breakthroughs in cooling and trapping techniques.

The time-dependent Hartree theory considers only the *coherent* part of the many-body problem. Of course, as is the case in conventional atom optics, the incoherent effects of spontaneous emission are expected to destroy the collective effects discussed above to some extent. We have now started to study the competition between coherent and incoherent effects as soon as we have a solid understanding of the coherent effects alone. This is an essential step both from a practical and a fundamental point of view. In particular, atomic solitons are mesoscopic quantum systems, which will permit us to study the transition from the microscopic, quantum world to the macroscopic classical world. It is now well understood that the survival of such systems over a reasonable time scale depends critically on their coupling to the environment. In the present case, this coupling is mainly via spontaneous emission.

The description of the combined coherent and incoherent effects is best performed in terms of a master equation, which includes both the effects of the vacuum field and of the laser fields with which the atoms are interacting. Specifically, one needs to derive an equation of motion for the effective single particle density operator $\bar{\rho}(2,1) = \langle\hat{\psi}^\dagger(1)\hat{\psi}(2)\rangle = Tr[\hat{\psi}^\dagger(1)\hat{\psi}(2)\rho]$, where ρ is the N-particle density operator. This equation can be derived by applying the Born-Markov approximation for the vacuum modes of the reservoir, and the Hartree-Fock approximation to factorize higher-order correlation functions of the form $\langle\hat{\psi}^\dagger(1)\hat{\psi}^\dagger(2)\hat{\psi}(3)\hat{\psi}(2)\rangle$ into products of second-order correlation functions, thereby introducing direct and exchange contributions. The resulting master equation contains the coherent contributions already present in the pure state Hartree approach. In addition, it contains a dissipative part that accounts for spontaneous emission and the concomitant atomic recoil as well as a nonlinear non-Hamiltonian term.

To properly assess the impact of spontaneous emission on the many-body effects that we discussed earlier, it is necessary to carry out numerical simulations, which are now underway. We also have initiated an effort to check the results of the effective single atom Hartree-Fock approach against "exact" results. For this reason, we also carry out explicit calculations with a small number of atoms, say two or three, using Monte Carlo wave function simulations.

REFERENCES

1. P. Verkerk, B. Lounis, C. Salomon, C. Cohen-Tannoudji, J.Y. Courtois and G. Grynberg, Phys. Rev. Lett. **68**, 3861 (1992).

2. P.S. Jessen, C. Gerz, P.D. Lett, W.D. Phillips, S.L. Rolston, R.C.J. Spreeuw and C.I. Westerbrook, Phys. Rev. Lett. **69** (1992).

3. P. Hemmerich and T.W. Haensch, Phys. Rev. Lett. **70**, 410 (1993).

4. G. Grynberg et al., Phys. Rev. Lett. **70**, 2249 (1993).

5. P.S. Julienne and F.H. Mies, J. Opt. Soc. Am. B **6** (1989).

6. J.W. Negele, Rev. Mod. Phys. **54**, 913 (1982).

7. G. Lenz, P. Meystre and E.M. Wright, Phys. Rev. Lett. **71**, 3271 (1993).

8. M. Prentiss et al., Opt. Lett. **13**, 452 (1988).

9. T. Walker, D. Sesko and C. Wieman, Phys. Rev. Lett. **64**, 408 (1990).

10. W. Ketterle et al., Phys. Rev. Lett. **70**, 2253 (1993).

Approved for public release;
distribution unlimited.

AIR FORCE OF SCIENTIFIC RESEARCH (AFSC)
NOTICE OF TRANSMITTAL TO DTIC
This technical report has been reviewed and is
approved for public release IAW AFR 190-12
Distribution in unlimited.
Joan Boggs
STINFO Program Manager